Please cite this articla as, "T. Tafsirojjaman, S. Fawzia, D. Thambiratnam, X. Zhao, Numerical investigation of CFRP strengthened RHS members under cyclic loading, Structures. 24 (2020) 610–626. doi:10.1016/j.istruc.2020.01.041.

Numerical investigation of CFRP strengthened RHS members under cyclic loading

T. Tafsirojjaman [a], Sabrina Fawzia [a,*], David Thambiratnam [a], Xiao-Ling Zhao [b]

[a] School of Civil Engineering and Built Environment, Faculty of Science and Engineering, Queensland University of Technology, 2 George Street, Brisbane, QLD 4000, Australia.

[b] Department of Civil and Environmental Engineering, The University of New South Wales (UNSW), Sydney, NSW 2052, Australia

([*]Corresponding author: sabrina.fawzia@qut.edu.au, Tel: 61731381012, Fax: 61 7 31381170

Email addresses: tafsirojjaman@hdr.qut.edu.au (T. Tafsirojjaman), sabrina.fawzia@qut.edu.au (Sabrina Fawzia), d.thambiratnam@qut.edu.au (David Thambiratnam), xiaolin.zhao@unsw.edu.au (Xiao-Ling Zhao)

ABSTRACT

Rectangular hollow section (RHS) steel members are commonly utilized in various mechanical and civil engineering applications, but they have shown to be quite vulnerable under cyclic loading. In both onshore and offshore infrastructure, steel members can be subjected to cyclic loading produced by earthquakes, currents, wind and waves. Considering multiple factors, such as design errors, the influence of environmental conditions, an increase in applied loads and material deterioration, steel members may require strengthening to withstand cyclic loadings. This study presents numerical simulations using Finite Element (FE) modelling techniques to analyse carbon fibre reinforced polymer (CFRP) strengthened RHS steel members subjected to cyclic loading to predict their behaviour and modes of failure. The predicted results are compared with available results from experimental tests to validate the numerical models and ensure their accuracy. Results imply that CFRP strengthened RHS steel members demonstrate enhanced cyclic performance in which the moment-rotation hysteresis behaviour, secant

stiffness and the energy dissipating capacity are improved compared those in bare steel RHS members. Furthermore, the effects of section thickness, bond length of CFRP, number of CFRP layers, wrapping orientation of CFRP and elastic modulus of CFRP on the response of these structural members are also investigated through detailed parametric studies.

Keywords: Rectangular Hollow Section (RHS) Steel members; Strengthening; CFRP; Finite element modelling; Cyclic loading.

1. Introduction

Rectangular hollow section (RHS) members have been a popular choice of both structural engineers and architects for use in steel frames and trusses in civil infrastructure. This popularity can be attributed to the advantages that RHS members have over other open members such as better corrosion resistance due to no sharp edges, higher fire protection capability and aesthetics [1]. Among natural disasters, earthquakes have been one of the leading causes of human casualties and property destruction. It is reported that there have been 1.87 million deaths due to Earthquakes in the 20^{th} century. Moreover, 2052 earthquake fatalities occurred during 1990-2010 [2]. Steel trusses and frames have been highly used for construction in seismic regions throughout the world, with these structures comprising primarily of RHS steel members. In particular, they have been used as structural elements in buildings as beams, columns and lattice girders and space frames in roofs. [1]. Failure of structural steel members under cyclic loads during the seismic events has become a major concern [3,4] in recent times. Such seismic damage to steel structures is not limited to land-based construction, with many offshore structures also prone to structural damage from earthquakes. This includes jacket-type structure which is extensively used in offshore construction where steel hollow members are welded together in the assembly of a space frame. This structure is often used to support platforms for the gas and oil industry. The dynamic loading imposed on these structures is greater than that on land-based structures as they also have to cope with loading from high

winds, waves and currents [4]. Worldwide, many steel structures are found to be lacking structural integrity due to incremental service loads, design errors, degradation of material properties and effects of severe environmental conditions. To rectify this problem there has been an increasing focus on research to improve the strength and rehabilitation of rectangular steel profiles to withstand high seismic excitations, but such research has been limited.

Traditional methods of rehabilitating steel structures have been through the process of welding additional bracing and plates to strengthen the structure. Although in theory, this process has structural benefits, certain key aspects of this process need to be taken into account such as the additional weight that is added to the structure as a result of the bracing and more importantly the introduction of heat-affected areas where members are added that change the distribution of stresses within the structure. These key aspects can be critical to structures that undergo fatigue loading, particularly in steel bridges. Furthermore, the resistance to corrosion can be compromised during this welding process. Additionally, to undertake this method of rehabilitation, heavy machinery and climbing equipment such as scaffolding are required, not to mention the long interruptions to the service of the building/structure across the duration of this process [4]. Alternatively by implementing the strength and rehabilitation process using carbon fibre reinforced polymer (CFRP) composites all of the aforementioned disadvantages can be avoided. The many advantages of using CFRP include high corrosion resistance [5], exceptional strength to weight ratio, tensile strength [6], cost efficiency as the process is less labour intensive with minimal preparation, can be easily applied in confined spaces as well as applied to any shape [7,8]. Previous research on CFRP strengthening has informed its ability to enhance the load-carrying capability [9], impact resistance capability [10] as well the ability to reduce the tip deflection in steel frame structures [11,12] under lateral loads. Furthermore, some research has also reported that CFRP strengthened members have higher resistance to local buckling [13,14] and higher capacity to absorb induced energy [15] than the original

members. One of the main advantages of CFRP strengthening is the improvement in the fatigue resistance of steel joints [16–18]. Considering all the above benefits in CFRP strengthening, an extensive numerical investigation has been undertaken with the focus on improving the structural performance of cantilevered RHS steel members subjected to cyclic loading during seismic excitation. The outcomes of this research will be helpful in restoring the structural integrity of steel members in high seismic regions by strengthening with CFRP.

Experimental and numerical research has been undertaken on the bending and hysteretic performance of tubular hollow members with externally applied CFRP reinforcement [9,19–21]. In their study, Kabir et al. found an increase of 37% in the load-carrying capability of CFRP strengthened circular hollow section (CHS) under pure four-point bending [9]. Previous research has also shown that the hysteretic behaviour of the CHS can be improved in terms of moment caring capacity, stiffness, energy dissipation capacity etc. due to the CFRP strengthening [21]. However, the structural responses of CFRP strengthened RHS members under cyclic loading has not been researched either experimentally or numerically. Given this gap in the research, there is little knowledge and understanding of CFRP wrapped RHS steel members under cyclic loading. With this in mind, this numerical study is focused on the lateral cyclic load response of RHS steel members strengthened with CFRP to predict their failure modes and overall behaviour. Numerical simulations have been performed by using the FE software ABAQUS CAE [22] and the modelling techniques have been validated by comparing the simulated results with published experimental results [21,23]. The performance of the CFRP strengthened models will be compared to that of the bare steel model in regards to moment-rotation hysteresis behaviour, secant stiffness and energy dissipation capabilities. Moreover, the effects of section thickness, the bond length of CFRP, the number of CFRP layers, wrapping orientation of CFRP and modulus of CFRP on the structural performance of the RHS members have been investigated with detailed parametric study. The outcome of this

paper is the provision of new information on the performance of CFRP strengthened RHS steel members that will benefit their intended applications.

2. FE modelling and validation

The FE model was created by using the ABAQUS CAE [22] to simulate the behaviour of CFRP strengthened RHS under cyclic loading. At first, the developed FE model is validated followed by parametric studies. The validation of the FE model is confirmed in a two-step process due to the unavailability of direct experimental results on cyclic behaviour of CFRP strengthened RHS. The first step is to validate the cyclic simulation process of RHS bare steel tubes with available cyclic test results [23]. Then, the second step is the validation of CFRP strengthening technique of steel members under cyclic loading using the results of tests conducted by the authors in a previous study [21]. Finally, the techniques from the above two validations are applied to CFRP strengthened RHS under cyclic loading to ensure accurate numerical simulation results.

2.1 Validation of Cyclic simulation process of bare RHS

The current numerical model is developed and validated by using the results from the experimental cyclic tests on HSS (including rectangular and square sections) carried out by Fadden [23]. The length of the rectangular hollow steel section (HSS) (i.e. RHS) 203×102×9.5 (mm) and 203×152×9.5 (mm) specimens in the FE model was taken as 1537 mm which is the same as the size of the experimental RHS specimen [23]. The geometrical details of the RHS sections were taken from the AISC Manual of Steel Construction [24]. The steel beam is created using 4-node shell elements (S4R) with reduced integration and hourglass control which is recommended for modelling the thin features. Mesh convergence study was conducted for the optimization of mesh size to confirm both the efficiency and accuracy of the FE model.

A nonlinear combined isotropic/kinematic hardening model was also applied as recommended to capture the inelastic hysteretic behaviour more accurately [25]. The material properties of steel for all of the FE models were obtained from the information provided by Fadden [23] with the modulus of elasticity, yield stress and ultimate strength of 181 GPa, 411 MPa, and 495 MPa respectively for the flats and 193 GPa, 517 MPa and 582 MPa respectively for the corners. Poison's ratio was assumed to be 0.3 for both the flats and corners.

The experimental cantilevered beams were fixed at the support end while the loading displacement was applied in the beam tip through a pin. In the experimental study AISC displacement control cyclic loading protocol [3], shown below in Figure 1(a) was applied in displacement control at a quasi-static loading rate. The reference point at the centre of the cross-section of both fixed end and the tip end of the beams was created and constrained all the peripheral nodes by multiple point constraints (MPC) as shown in Figure 1(b). Boundary conditions of the experiment were replicated by making all translational and rotational degrees of freedom fixed and free for the support and tip reference points respectively. The fixed end of the HSS was sandwiched between two large angles to provide a reusable connection during the experimental study [23] and there was some flexibility in the connection. Hence, it was observed that each section underwent some amount of rigid (body) rotation at the connection [23]. At the highest displacement of each cycle, the measured rigid rotation was subtracted from the overall measured rotation, leaving the actual rotation due to the deformation of the HSS members [23]. Then, models were then placed under the exact same displacement control cyclic loading protocol [3] that each experimental specimen underwent with rigid rotations removed [23] at the tip reference point to simulate the cyclic behaviour of the RHS. Hence, the FE model could simulate the flexibility at the highest displacements and showed a good agreement at the ultimate rotational regions. Unfortunately, this was not possible for regions in between the highest positive and highest negative regions as no data was available on when

and how much of flexibility was mobilised in these regions. Due to this limitation of information, in these regions specially the reloading area showed small deviations between numerical and experimental results.

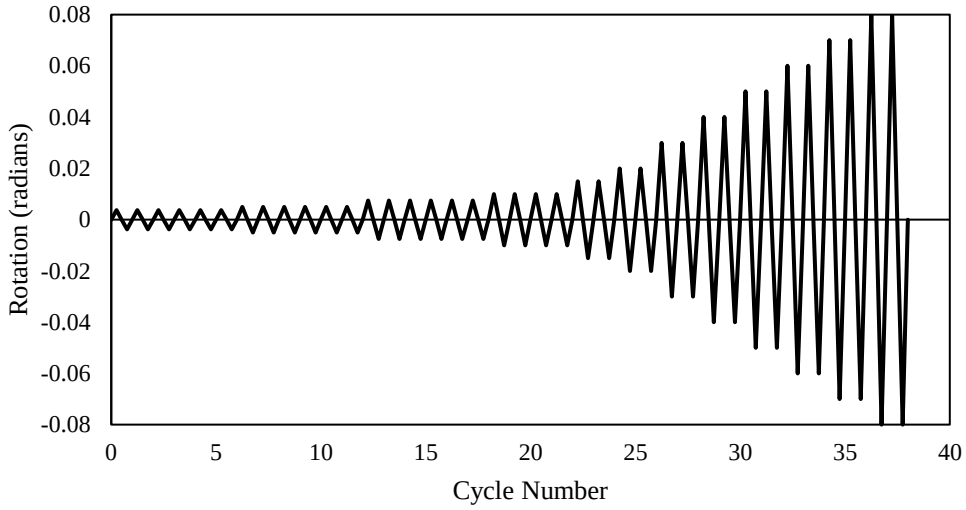

(a)

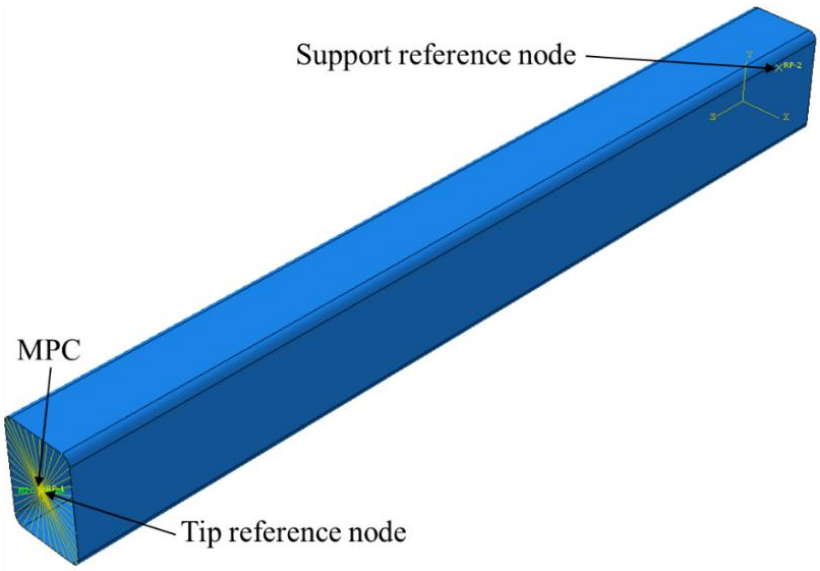

(b)

Figure 1: (a) Quasi-static cyclic loading protocol [3] and (b) Boundary conditions

The developed FE model was then validated by comparing the simulated moment versus rotational hysteresis, normalized moment versus rotational backbone and secant stiffness

versus rotational results with the available experimental results [23]. In the present study, the moment was measured by multiplying the simulated load by the beam length of 1537 mm. The normalized moment versus rotational backbone curves obtained by plotting the normalized moment against the highest rotation of every cycle. The normalised moment was calculated by dividing the experimental moment by the calculated plastic moment. In addition, the secant stiffness of a particular (singular) rotation was obtained by dividing the load at the highest displacement of that particular rotation by the highest displacement of that particular rotation. Figure 2 and Figure 3 show a good agreement of moment-rotation hysteresis and normalized moment-rotation hysteresis backbone curves respectively obtained from the tests and the FE analyses although a small deviation from the experiments were observed in the reloading area due to lack of information about the flexibility in this region.The overall maximum moment capacity of FE models for the 203×102×9.5 (mm) and 203×152×9.5 (mm) were 170 kN.m and 197 kN.m which were only 1.55% higher and 2.96% lower than the experimental overall maximum moment capacities respectively. Moreover, the well-matched secant stiffness versus rotation curves in Figure 4 confirms the accuracy of the present FE models for the cyclic simulation process

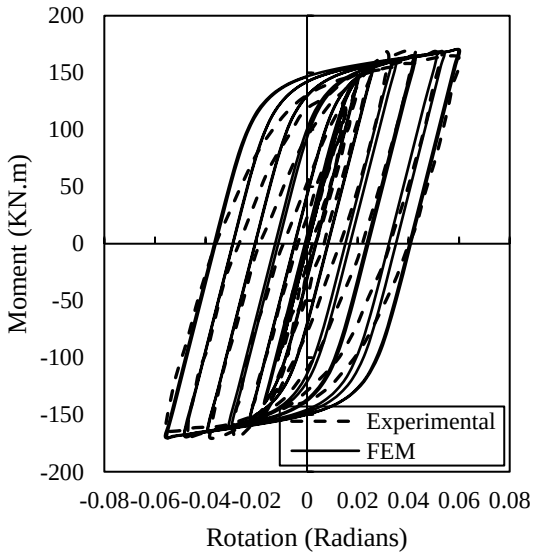

(a)

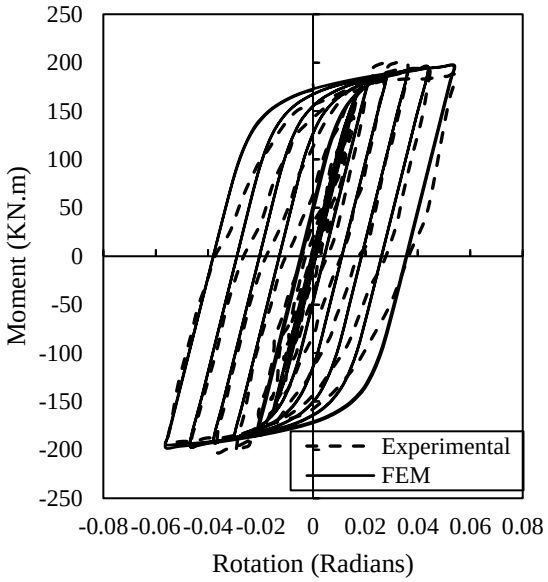

(b)

Figure 2: Experimental and FE model moment-rotation hysteresis curves for (a) 203×102×9.5 and (b) 203×152×9.5.

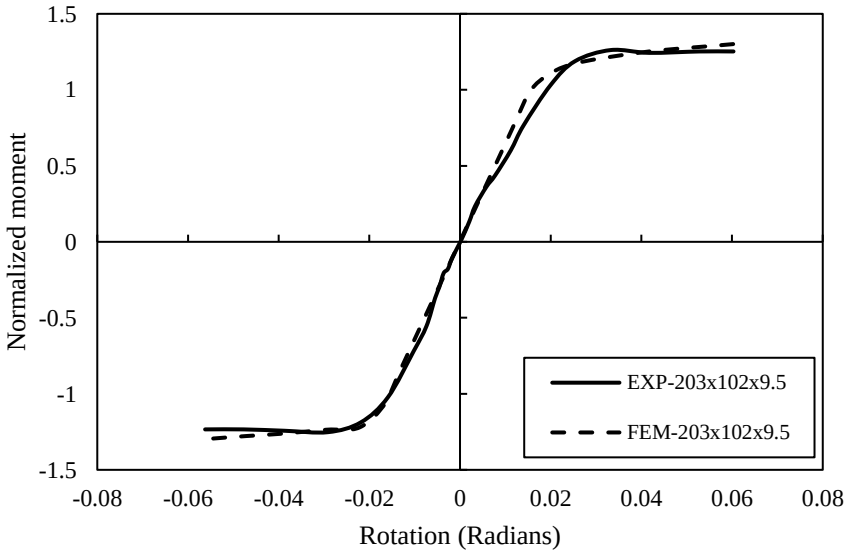

(a)

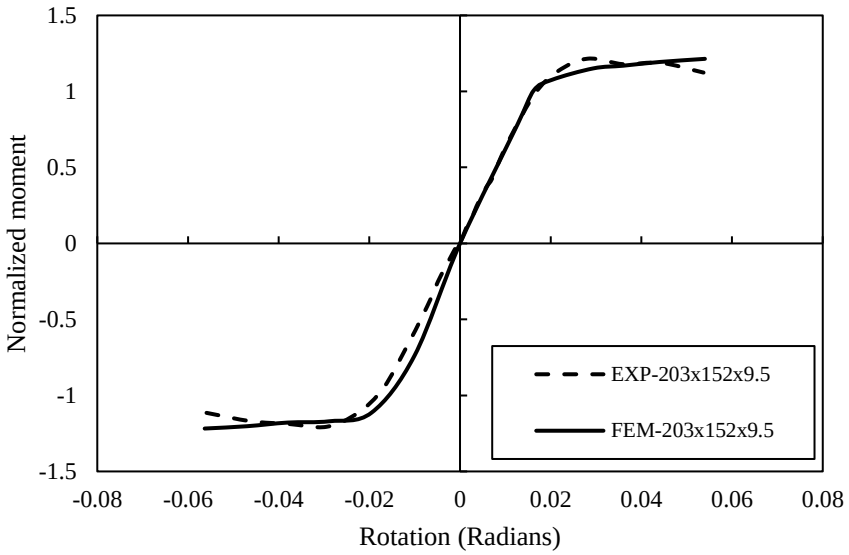

(b)

Figure 3: Experimental and FE model normalized moment versus rotation backbone curves for (a) 203×102×9.5 and (b) 203×152×9.5.

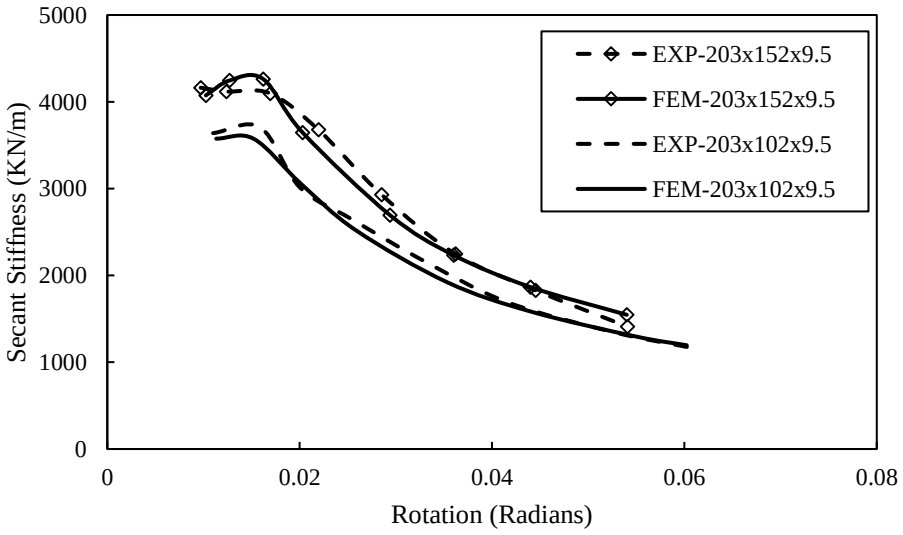

Figure 4: Experimental and FE model secant stiffness versus rotation curves for 203×102×9.5 and 203×152×9.5.

2.2 Validation of the FE model of CFRP strengthened steel member

2.2.1 FE modelling and element types

The FE model of CFRP strengthened Circular Hollow Section (CHS) steel member has been developed and validated using available experimental results [21]. Information on the specimen and experimental setup can be found in Tafsirojjaman et al. [21]. Using the same FE software as in previous section 2.1, ABAQUS [22], 3D finite element model of CFRP strengthened CHS steel member was developed with external diameter, wall thickness and length of 101.6 mm, 4 mm and 1100 mm respectively to replicate the experimental specimen [21].

In the FE model, the adhesive and CFRP were applied for a bond length of 900 mm from the fixed end. Fibre orientations of the three layers of CFRP were kept the same LHL (longitudinal, direction, hoop direction and again longitudinal direction respectively) as in the experiment to simulate the test members. Several previous studies [26,27] demonstrate that the general thickness of adhesives range from 0.1 to 0.3mm and hence, 0.1 mm thickness is assumed for the adhesive layer in this study. As the debonding between CFRP-CFRP layers was not evident during the experiment, the adhesive was modelled in the interface between the surface of the steel member and the first (innermost) CFRP layer only and delamination was simulated between CFRP and steel surface if any.

The experimental cantilevered members were fixed at the support end while the loading displacement was applied in the beam tip through a pin. In the experimental study AISC displacement control cyclic loading protocol [3] was adopted and applied in displacement control at a quasi-static loading rate. At the centre of the cross-section of both end of CHS member, an independent reference node was created and all the peripheral (circumferential) nodes of the member were modelled as constrained to this reference node using beam type multiple point constraint (MPC). The supported end reference point was set to be fully fixed

which means that all translational and rotational degrees of freedom were fixed. In contrast, the member tip reference point was set to be free in translational and rotational degrees of freedom to represent the experimental setup. [21]. In addition, the tip reference point was created 1200 mm far from the fixed end as the cyclic load was applied in 1200 mm far from fixed end in the experiment. Then, the same experimental displacement control cyclic loading as described in experimental study [21] was applied at the tip reference point to simulate the cyclic behaviour of the CFRP strengthened CHS.

The steel section is modelled by using the same elements as in the previous validation section 2.1 i.e. 4-node shell elements (S4R) with reduced integration and hourglass control. Mesh convergence study was carried out to ensure the accuracy and efficiency of the FE model. To predict the adhesive behaviour and failure modes, 3-D cohesive elements (COH3D8) were utilized for the adhesive layer [27–30]. 8-node quadrilateral continuum shell elements (SC8R) with reduced integration and hourglass control were used to model the CFRP layers. Previous researchers concluded that continuum shell elements are most appropriate to model CFRP composition due to the capability of accurately predicting the CFRP composite failure [27–30]. Both continuum and cohesive elements are modelled via offsetting an orphan mesh that is allocated in the outward stacking direction. To assign the orientation of CFRP, different sections were modelled for each of transverse and longitudinal CFRP layers. The orphan nodes were sheared to connect between the all interacting surfaces of adhesive and CFRP layers, while the tie constraint was applied to initialize the bonding of CFRP composites with the external surface of the steel tube.

2.2.2 Material model and properties

2.2.2.1 Steel

The validated material model for steel in the previous section 2.1 was used for modelling steel to maintain consistency in the FE modelling. Material properties of steel were obtained from the available experimental study [21] and the yield stress, ultimate tensile strength and the modulus of elasticity of steel were 320 MPa, 367 MPa and 190 GPa respectively, while Poison's ratio was assumed to be 0.3.

2.2.2.2 Adhesive

To simulate the traction between the steel surface and CFRP, the adhesive layer was applied using a coupled cohesive zone which obeys traction separation law where all three directional tractions and separations have been considered. They are the normal direction and two parallel directions as shear components. Normal and shear tractions are denoted by t_n, t_s and t_t, while the separations are denoted by δ_n, δ_s and δ_t respectively.

Before damage in the adhesive initiated, the response of adhesive is assumed to be linear [31–34]. Thus, the interfacial behaviour of the adhesive before damage initiation is represented by,

$$\begin{bmatrix} t_n \\ t_s \\ t_t \end{bmatrix} = \begin{bmatrix} k_{nn} & 0 & 0 \\ 0 & k_{ss} & 0 \\ 0 & 0 & k_{tt} \end{bmatrix} \begin{bmatrix} \delta_n \\ \delta_s \\ \delta_t \end{bmatrix} \quad (1)$$

In the above equation $k_{nn,}\, k_{ss}$ and k_{tt} denote the elastic stiffness in the normal and shear directions respectively. The mode-I failure controls the normal direction, while the mode-II failure controls the shear directions. The stiffness k_{nn} is determined from the initial slope of the bond separation model for mode-I loading.

$$k_{nn} = \frac{E_a}{T_o} \tag{2}$$

where E_a and T_o represent the elastic modulus and the adhesive thickness (0.1 mm) respectively. It was assumed that k_{ss} and k_{tt} are equal to the initial slope of the mode-II loading [30] and they are given by,

$$k_{ss} = k_{tt} = 3\left(\frac{G_a}{T_0}\right)^{0.65} \tag{3}$$

where G_a denotes the shear modulus and can expressed as $G_a = \frac{E_a}{2(1+\nu)}$ [9] where ν is the Poisson's ratio of adhesive and the value is 0.39 [35]. The adhesive requires a sufficient stiffness value to provide sensible stiffness, however, a stiffness that is too big could initiate oscillations in the interface [9]. The initial stiffness parameters, k_{nn}, k_{ss} and k_{tt} cannot be measured directly through the experiment; however Eqs. (2) and (3) also give a reasonable initial approximation for k_{nn}, k_{ss} and k_{tt}. Therefore, in order to find a reasonable estimation of k_{nn}, k_{ss} and k_{tt} various numerical simulations with different k_{nn}, k_{ss} and k_{tt} values need to be compared to the experimental results [9,36]. The present values of k_{nn}, k_{ss} and k_{tt} are obtained from the one of authors previous study [9] where same adhesive was used and is given in Table 1.

In the present FE model, the definition of damage initiation of adhesive is based on QUADS failure criteria where the loading effects from both mode-I and mode-II are considered (Equation 4). When the function achieves a value of 1 unit, the damage will be initiated [22]. The symbol '⟨⟩' denotes that t_n, t_s and t_t are set to zero when the adhesive is under compression as compressive stressed are assumed not to cause damage.

$$\left\{\frac{\langle t_n \rangle}{\sigma_{\max}}\right\}^2 + \left\{\frac{\langle t_s \rangle}{\tau_{\max}}\right\}^2 + \left\{\frac{\langle t_t \rangle}{\tau_{\max}}\right\}^2 = 1 \quad (4)$$

In the equation $\sigma_{\max}$ and $\tau_{\max}$ denotes the maximum stresses in the opening direction (mode I), sliding direction (mode II) and tearing direction (mode III) of the contact. As the adhesive is an isotropic material the value of $\sigma_{\max}$ and $\tau_{\max}$ are assume same according to Kabir et al. [9].

When the damage initiation condition is reached, the degradation of the material stiffness starts and the evolution of damage begins. The phenomenon of damage evolution has been modelled based on linearizing energy softening mechanism in ABAQUS in which Benzeggah-Kenance fracture energy based mixed mode law was applied (Equation 5) [37].

$$G_I + (G_{II} - G_I)\left(\frac{G_s}{G_t}\right)^{\eta} = G_n \quad (5)$$

where, G_I and G_{II} denote the maximum fracture energies in normal and shear directions, which cause the failures in normal and shear directions respectively, whereas G_n, G_s and G_t denote the corresponding work done. Values for G_I and G_{II} are obtained from Alam et al [27]. The adhesive properties are given in Table 1.

Table 1: Material properties of adhesive

Parameter	Value
E_a	2.86 GPa
$\sigma_{\max}$	46 MPa
k_{nn}	2.8×10^{13} N/m^3
$k_{ss} = k_{tt}$	1.4×10^{13} N/m^3
G_I	1000 N/m
G_{II}	1250 N/m

2.2.2.3 CFRP

Lamina elastic material was used to model the CFRP composite, whilst the composite damage in the simulation was taken as failure criteria in Hashin [38,39]. This model was adopted as it has the capability of accurately predicting the elastic-brittle damage related to CFRP [40]. Four alternative failure modes of CFRP were considered in this model, listed as: i. F_f^t – rupture of fibre in tension, ii. F_f^c – buckling of fibre in compression, iii. F_m^t – transverse shearing and tension matrix cracking, iv. F_m^c – transverse shearing and compression matrix cracking. The following equation was adopted for the model whereby values of one or higher represent the initiation of damage for that singular failure mode.

$$F_f^t = \left(\frac{\sigma_{11}}{T^L}\right)^2 + \alpha\left(\frac{\sigma_{12}}{S^L}\right)^2$$

$$F_f^c = \left(\frac{\sigma_{11}}{C^L}\right)^2$$

$$F_m^t = \left(\frac{\sigma_{22}}{T^T}\right)^2 + \left(\frac{\sigma_{12}}{S^L}\right)^2$$

$$F_m^c = \left(\frac{\sigma_{22}}{2S^T}\right)^2 + \left[\left(\frac{\sigma_{12}}{2S^T}\right)^2 - 1\right]\frac{\sigma_{22}}{C^T} + \left(\frac{\sigma_{12}}{S^L}\right)^2 \quad (6)$$

where, C, T and S represent compressive, tensile and shear strength respectively, while longitudinal and transverse directions are represented by subscripts L and T. Additionally, the contribution of shear stress (taken as 1.0) is denoted by 'α' whilst stress tensor components are represented by σ_{11}, σ_{22} and σ_{12} respectively. Once damage initiation and evolution have occurred for at least one mode, the damage operator becomes significant in the criteria for damage initiation of other modes [22]. An output variable is associated with each initiation criterion (fiber tension, fiber compression, matrix tension, matrix compression) to indicate

whether the criterion has been met. A value of 1.0 or higher indicates that the initiation criterion has been met [22]. Moreover, when the amount of energy dissipated equals the energy for critical fracture of a given failure mode, the damage criteria are achieved and initiate the damage evolution. Therefore for each failure mode in the FE model, critical fracture energies need to be given.

The elastic modulus (E_{IC}) and average tensile strength (T^L) are taken from the available experimental study [9,21]. Moreover, the fracture energies for individual failure criterion were taken from Faggiani et al. [41] and given in Table 2. Fracture energy is denoted by G while subscripts m, f, c and t denote the matrix, fibre, compression and tension respectively. The variation of the compressive strength (C^L) of common CFRP types is 9-60% of its corresponding tensile strength [42,43]. Therefore, the longitudinal compressive strength of the CFRP was taken as 20% of the tensile strength while the transverse tensile/compressive and longitudinal/transverse shear strengths were assumed as 10% of the tensile strength according to Imran et al. [28]. Various research has indicated that this assumption falls within an accurate range [40,41]. Poison's ratio of 0.33 was adopted for the CFRP. Figure 5 shows the details of FE modelling.

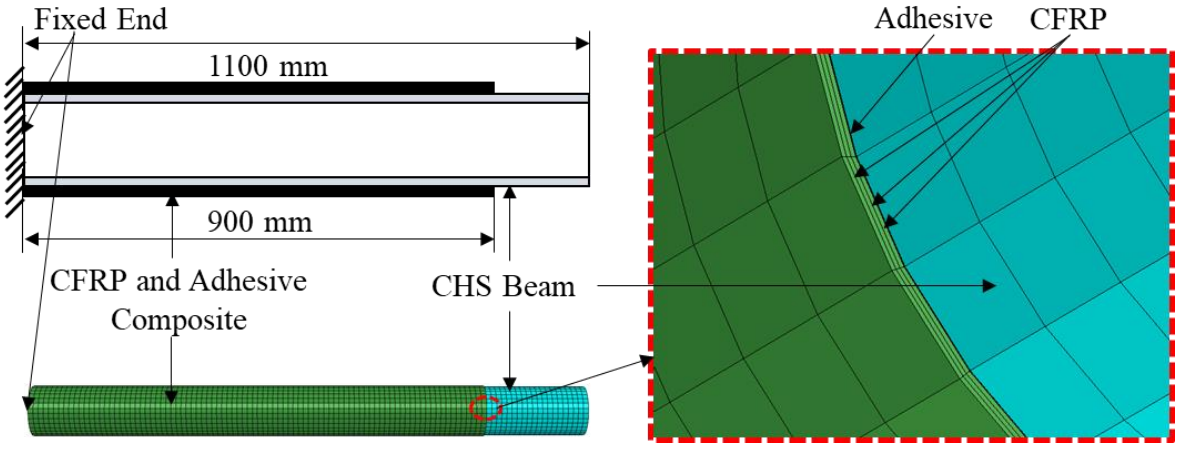

Figure 5: Details of FE modelling

Table 2: Material properties of CFRP

Parameter	Value
E_{1C}	75 GPa
E_{2C}	25 MPa
T^{L}	987 MPa
G_{ft}	91,600 N/m
G_{fc}	79,900 N/m
G_{mc}	1100 N/m
G_{mt}	220 N/m

2.2.3 Validation

The FE simulated moment versus rotational hysteresis, moment versus rotational backbone and secant stiffness versus rotational results were compared with the available experimental results [21] to confirm the validation of the FE models of CFRP strengthened steel members. Figure 6 and Figure 7 show a good agreement of moment versus rotational hysteresis and moment versus rotational backbone curves respectively between experimental and FE simulated results although a small deviation from the experiments were observed in the reloading area due to lack of information about the flexibility in this region.The overall maximum moment capacity of FE models for the CFRP strengthened steel member was 16.8 kN.m which was only 1.75% lower than the experimental overall maximum moment capacity of 17.1 kN.m. Moreover, the well-matched secant stiffness versus rotation curves in Figure 8 confirms the accuracy of the present FE model of the CFRP strengthened steel member.

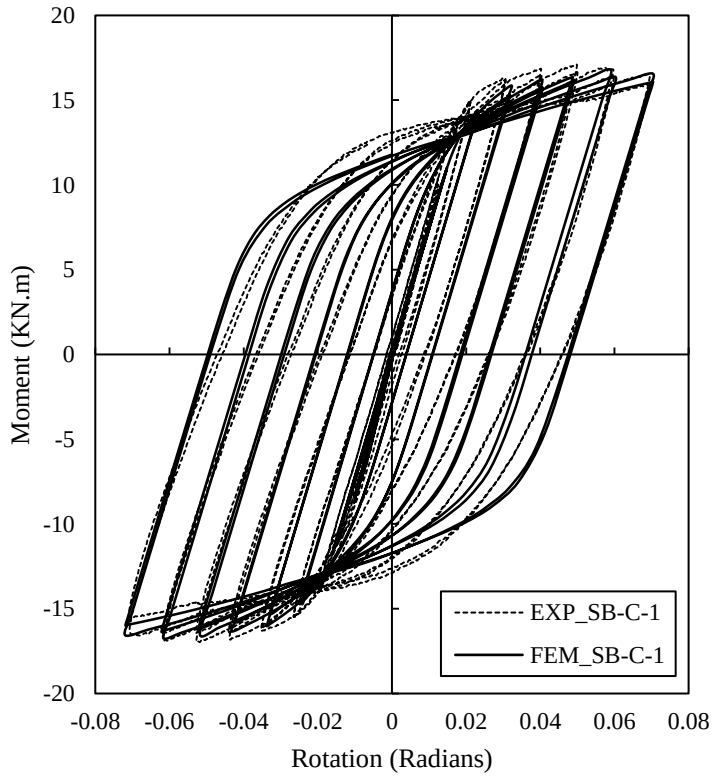

Figure 6: Experimental and FE model hysteresis curves of the CFRP strengthened steel member (SB-C-1).

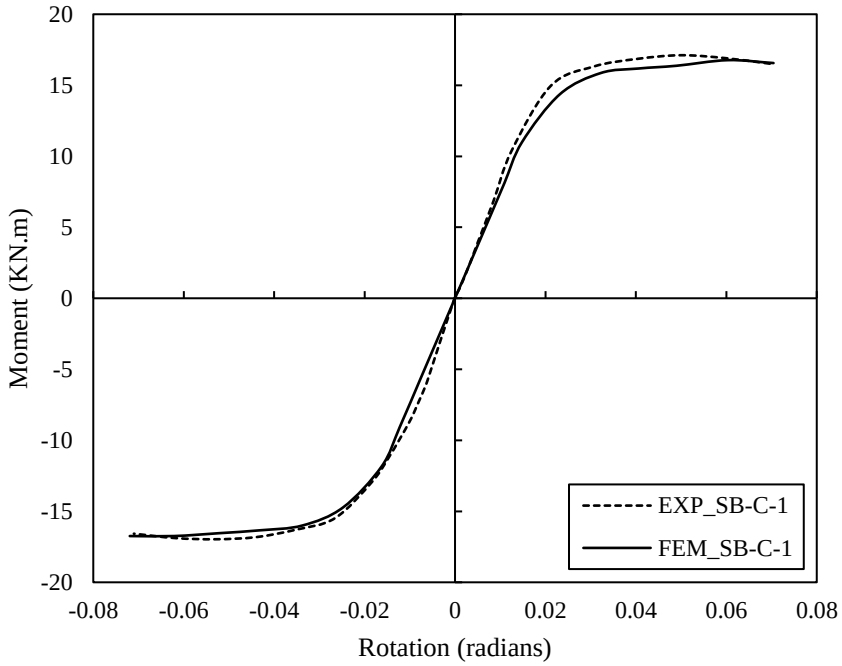

Figure 7: Experimental and FE model moment versus rotational backbone curves of the CFRP strengthened steel members (SB-C-1).

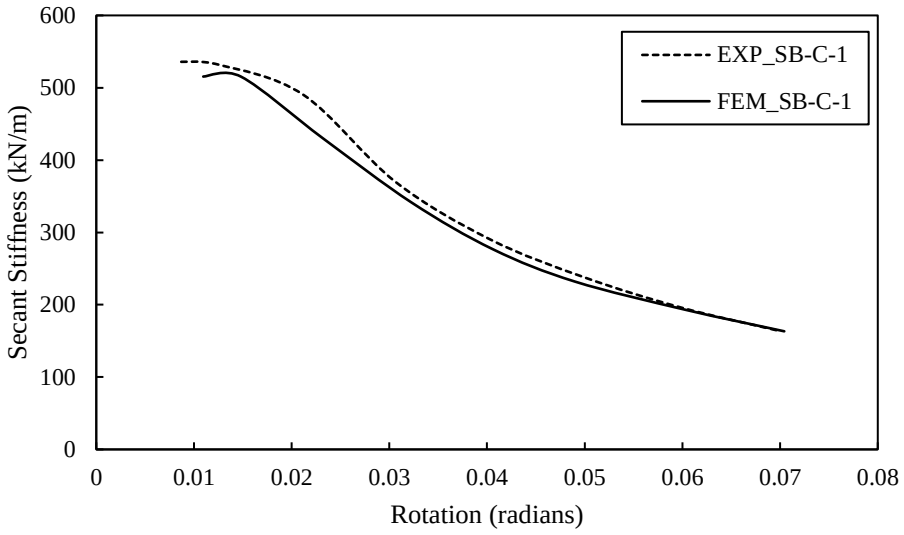

Figure 8: Experimental and FE model secant stiffness versus rotational curves of the CFRP strengthened steel member (SB-C-1)

3. Cyclic Simulation of CFRP strengthened RHS

Behaviour of CFRP strengthened RHS members under cyclic loading has not yet been investigated and hence there are no experimental data on CFRP strengthened RHS subjected to cyclic loading. This paper therefore simulates the behaviour of CFRP strengthened RHS members under cyclic loading using the developed FE model based on validated FE models of bare RHS and CFRP strengthened steel members. First, the FE model of bare RHS members of 1537 mm length was developed using the same steel properties and (validated) modelling techniques described in section 2.1. Then, the bare RHSs were strengthened with CFRP using the same CFRP and adhesive material properties and validated CFRP strengthening techniques described in the previous section 2.2. Finally, the cyclic analysis is conducted on CFRP strengthened RHS members to simulate the behaviour of CFRP strengthened RHS members under cyclic loading by following the validated cyclic simulation process to ensure accurate numerical simulation. Figure 9 shows the details of the FE model of CFRP strengthened RHS member.

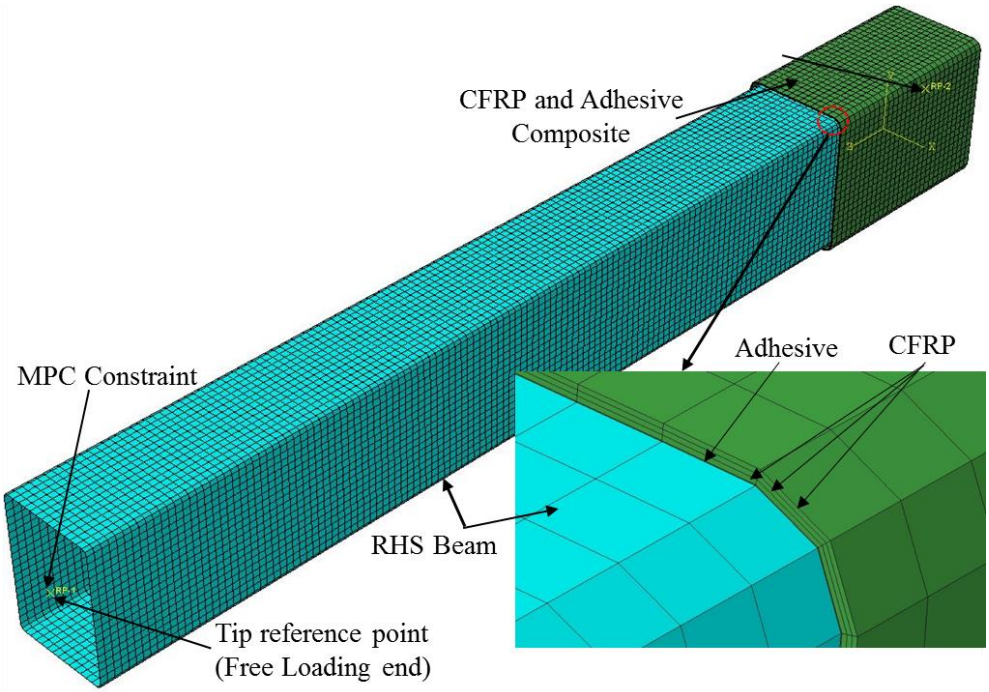

Figure 9: Details of FE model of CFRP strengthened RHS member

4. Parametric Study on CFRP strengthened RHS

The numerical study on the behaviour of CFRP strengthened RHS members under cyclic loading has been conducted by utilizing the validated FE models. A detailed parametric study is carried out to evaluate the effects of section thickness, the bond length of CFRP, the number of CFRP layers, wrapping orientation of CFRP and modulus of CFRP on the structural performance of the modelled members under cyclic loading. The behaviours of the CFRP strengthened RHS members are investigated in regards to moment-rotation hysteresis behaviour, secant stiffness and energy dissipation capabilities.

4.1 Effects of the thickness of RHS

Three RHS members are considered with constant cross-sectional width and height but with different wall thicknesses of 4.8 mm, 7.9 mm and 9.5 mm (203×152×4.8 (mm), 203×152×7.9 (mm) and 203×152×9.5 (mm) respectively) to evaluate the effect of RHS thickness. All these RHSs were strengthened with three layers of CFRP and 300 mm bond length from the fixed

end. Moment-rotation hysteresis and moment-rotation backbone curves of bare and CFRP strengthened RHS members were developed to assess the bending behaviour and the cyclic hysteresis responses of the bare and CFRP strengthened RHS members. Comparisons of the moment-rotation hysteresis curves for the bare and CFRP strengthened RHS members are shown in Figure 10(a), Figure 10(b) and Figure 10(c) for the 203×152×9.5 (mm), 203×152×7.9 (mm) and 203×152×4.8 (mm) respectively. Overall, both of the bare and CFRP strengthened RHS members exhibited the appropriate inelastic behaviour by displaying the full hysteretic loops. Moreover, the moment versus rotation backbone curves of the bare and CFRP strengthened RHS members for the 203×152×9.5 (mm), 203×152×7.9 (mm) and 203×152×4.8 (mm) are shown in Figure 11. It is clear from these Figures that both the bare and CFRP strengthened RHS members display a good symmetry in both positive and negative cycles which ensure stable responses for both rotations. In addition, it can be seen that strengthening of RHS by CFRP is very effective as a good enhancement of moment capacity has been found for CFRP strengthened RHS members compared to the bare RHS members. CFRP strengthened 203×152×9.5 (mm), 203×152×7.9 (mm) and 203×152×4.8 (mm) members showed higher moment capacities of 217 kN.m, 188.25 kN.m and 115.07 kN.m respectively, compared to the moment capacities of 197.76 kN.m, 165.14 kN.m and 97.16 kN.m shown by the bare 203×152×9.5 (mm), 203×152×7.9 (mm) and 203×152×4.8 (mm) members respectively. Hence, as a result of the CFRP strengthening, the moment capacities have been enhanced by 9.72%, 14% and 18.44% for the RHS members with 9.5 mm, 7.9 mm and 4.8 mm section thickness respectively. In addition, it can be concluded from the moment versus rotational hysteresis and moment versus rotational backbone curves that the CFRP strengthened RHS members have exhibited a better moment degradation behaviour than the bare RHS members for all sections. Moreover, the effectiveness of CFRP to enhance the cyclic

behaviour of RHS members is increasing with the decreasing the thickness of RHS as the ratio of CFRP thickness to RHS thickness is increased.

Figure 12 shows the comparison of the secant stiffness-rotation curves for the bare and CFRP strengthened RHS members with different wall thicknesses. It is evident that the strengthening of RHS by CFRP is also effective in terms of secant stiffness as a reasonably good enhancement of secant stiffness is shown by the strengthened RHS members under cyclic loading. Overall, both bare and CFRP strengthened RHS members exhibit a decreasing order of secant stiffness with increasing rotation. At the ultimate capacity rotational level (as in Figures 11), the CFRP strengthened 203×152×9.5 (mm), 203×152×7.9 (mm) and 203×152×4.8 (mm) members showed the higher secant stiffness of 1717 kN/m, 1477 kN/m and 1746 kN/m respectively (Figure 12), whereas the bare 203×152×9.5 (mm), 203×152×7.9 (mm) and 203×152×4.8 (mm) members showed a lower secant stiffness of 1546 kN/m, 1150 kN/m and 1209 kN/m respectively (as seen from the same Figures). Hence, as a result of the CFRP strengthening, the secant stiffness has been enhanced by 11.05%, 28.44% and 44.42% for the RHS members with 9.5 mm, 7.9 mm and 4.8 mm section thickness respectively. Moreover, the CFRP strengthened RHS members showed a lower secant stiffness degradation compared to the bare RHS members, although both of them exhibited quite the same trend of the degradation of secant stiffness. At the maximum rotational level, the CFRP strengthened RHS members with the wall thickness of 9.5 mm, 7.9 mm and 4.8 mm, the secant stiffness was reduced from their maximum values by 63.86%, 64.79% and 82.83% respectively , while for the bare RHS members they were 66.45%, 71.71% and 85.9% respectively.

The energy dissipation versus rotation curves of the bare and CFRP strengthened RHS members for the 203×152×9.5 (mm), 203×152×7.9 (mm) and 203×152×4.8 (mm) are shown in Figure 13. The energy dissipation capacity in a cycle is obtained by calculating the enclosed area of the particular hysteresis loops of that cycle. Then, the accumulative energy dissipation

of all cycles at that particular rotational level is shown in Figure 13. In general, the ability to dissipate energy by both bare and the CFRP strengthened RHS members can be confirmed as they are capable of generating the full hysteresis curves. Before yielding i.e. up to the small rotational level of 0.015 rad., the energy dissipation capacity of both bare and the CFRP strengthened RHS members remained very small as the members behaved essentially elastic. For the largest wall thickness of 9.5 mm of the RHS member, the bare specimen had sufficient stiffness at the end of the present rotation and this explains why there was no contribution from the CFRP stiffness to increase the energy dissipation capacity. Hence, the energy dissipation capacities were almost the same at the maximum rotational level for both the bare and CFRP strengthened RHS with 9.5 mm wall thickness, while for the RHS members with the smaller wall thickness of 7.9 mm and 4.8 mm, strengthened members showed 27.6% and 21.4% higher energy dissipation capacities than the bare members.

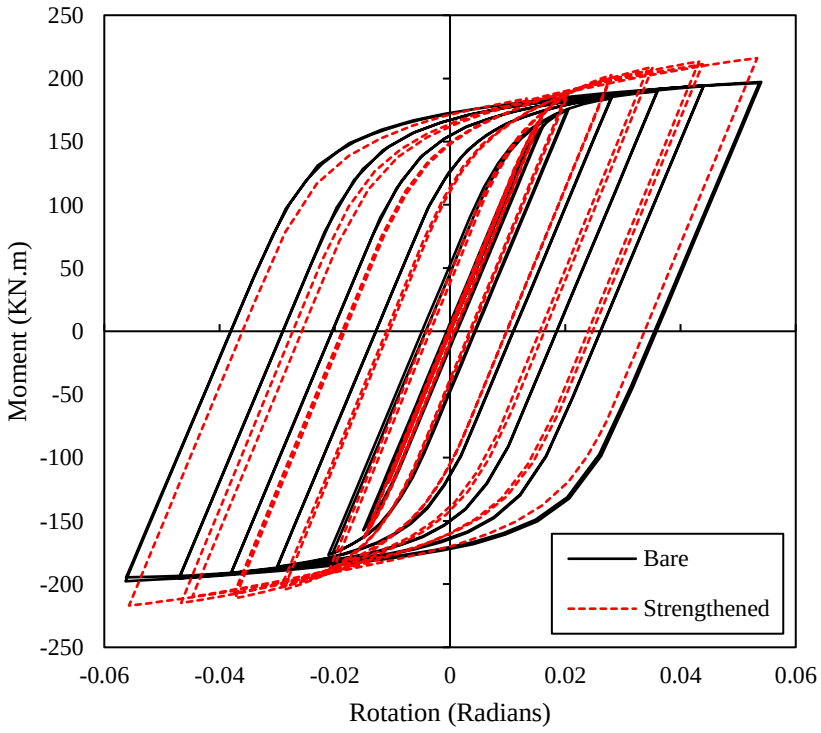

(a)

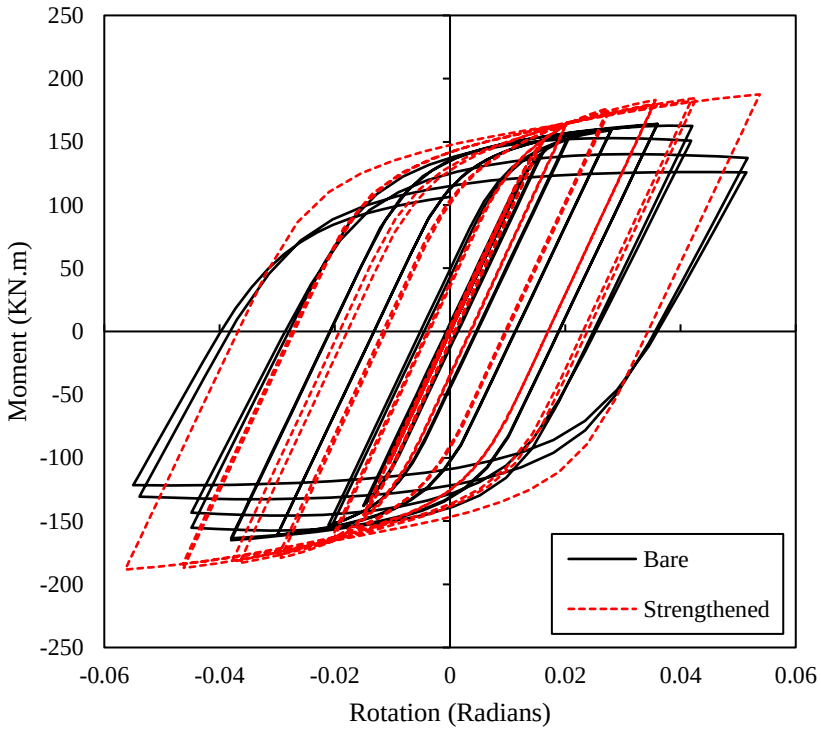

(b)

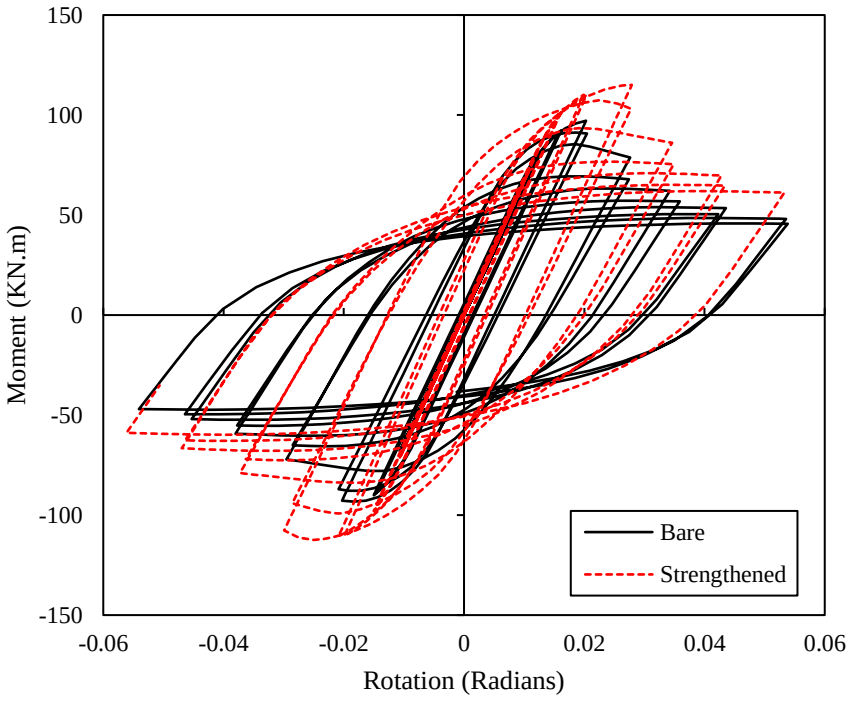

(c)

Figure 10: Moment-rotational hysteresis curves of the bare and CFRP strengthened RHS members for (a) 203×152×9.5 and (b) 203×152×7.9 and (c) 203×152×4.8.

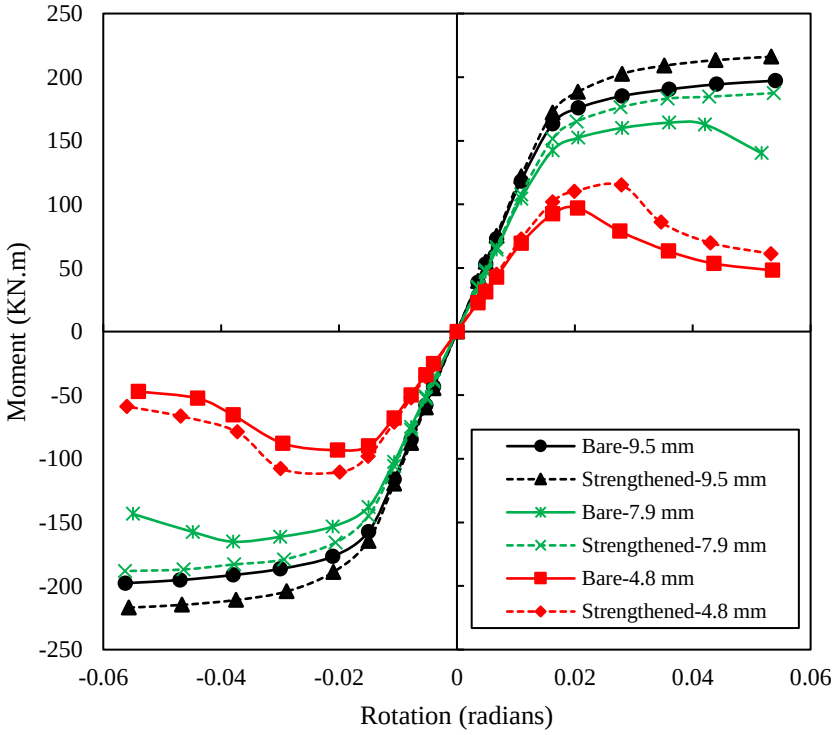

Figure 11: Moment-rotational backbone curves of bare and CFRP strengthened RHS members with different wall thicknesses

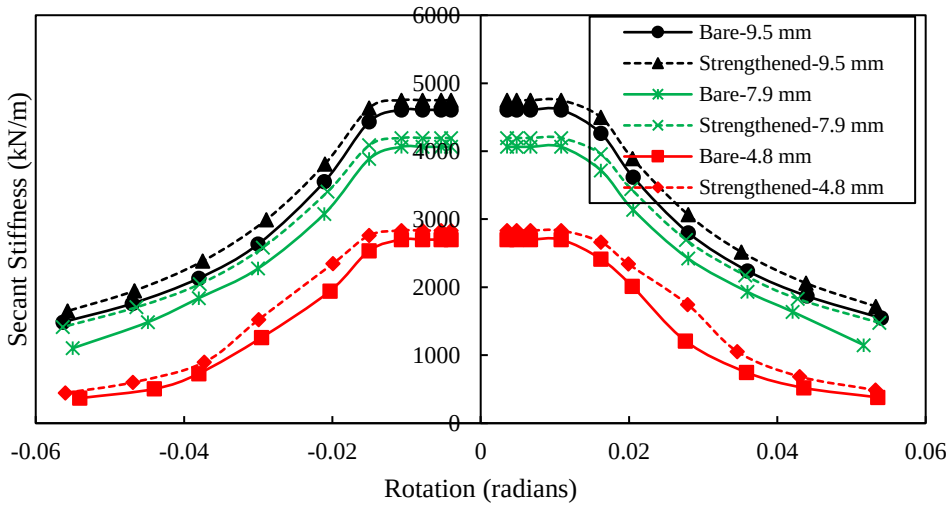

Figure 12: Secant stiffness-rotational curves of the bare and CFRP strengthened RHS members with different wall thicknesses.

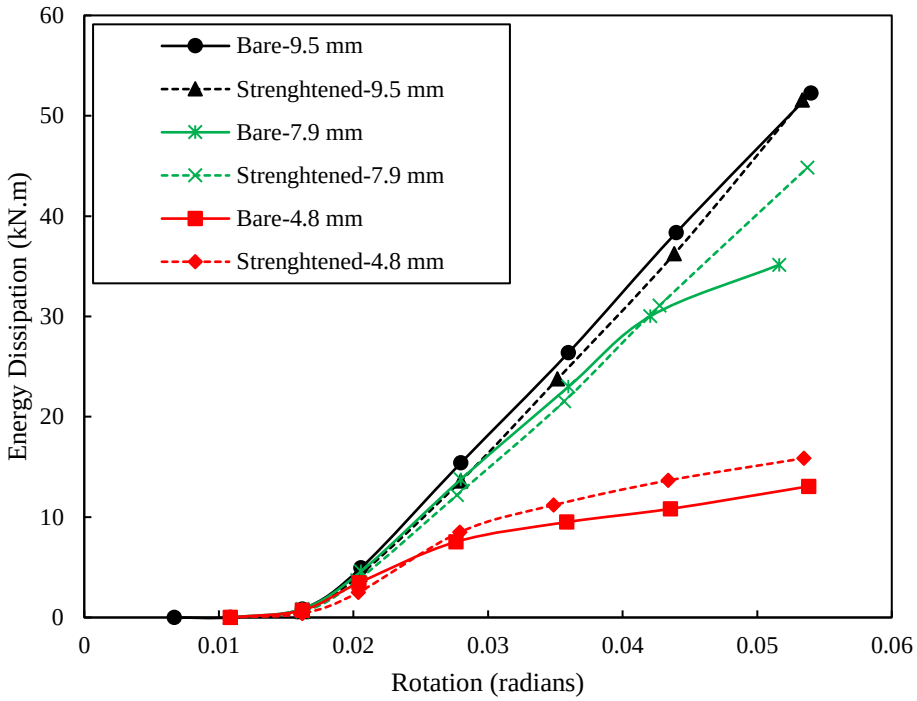

Figure 13: Energy dissipation-rotational curves of bare and CFRP strengthened RHS members with different wall thicknesses.

4.2 Effects of bond length of CFRP

The effect of CFRP bond length on the behaviour of CFRP strengthened RHS members under cyclic loading was investigated by varying the wrapping length of the CFRP. This information is very important in the CFRP strengthening technique in order to minimize the civil engineering project cost. The main aim here is to ascertain the most cost-effective bond length but the strengthened RHS should be structurally sound. 203×152×4.8 (mm) was considered to determine the effect of CFRP bond length. RHS members wrapped with different bond lengths of 150 mm, 250 mm, 300 mm and 350 mm of CFRP were considered. Moment-rotation backbone curves, maximum moment capacities, secant stiffness-rotation curves and the energy dissipations of CFRP strengthened RHS members with different bond lengths of CFRP are compared in Figure 14, Figure 15, Figure 16 and Figure 17 respectively.

From Figure 14-Figure 17, it can be seen that there are small but steady improvement of different response characteristics (maximum moment capacity, moment degradation, secant stiffness and energy dissipation) when the bond length is increased from 150-250 mm. When the bond length is increased from 250-300 mm there is a greater enhancement in all these response parameters. However, very little or no change in these response parameters is observed after increase in bond length beyond 300 mm. Maximum moment capacities of CFRP strengthened RHS members with 150 mm, 250 mm, 300 mm and 350 mm CFRP bond lengths improved by 5.63%, 11.92%, 18.44% and 20.51% respectively compared to those of bare RHS member. CFRP strengthened RHS members with 300 mm and 350 mm CFRP bond lengths show almost the same moment degradation behaviour and better than that of CFRP strengthened RHS members with 150 mm and 250 mm CFRP bond lengths. Moreover, at the end rotation, CFRP strengthened RHS members with 150 mm, 250 mm, 300 mm and 350 mm bond lengths show improvements in secant stiffness of 18.81%, 25.84%, 41.10% and 47.14% respectively, and enhanced energy dissipation capacities of 4.94%, 12.67%, 17.82% and 18.78% respectively compared to bare RHS member.

The failure modes of CFRP strengthened RHS members with the different CFRP bond lengths are shown in Figure 18. In the CFRP strengthened RHS members with bond length of 150 mm, 250 mm and 300 mm, local buckling has shifted from the support end to the steel beyond the CFRP wrapped area, while the local buckling occurs at the support end for the CFRP strengthened RHS member with 350 mm bond length and further shifting of local buckling will not be possible beyond 300 mm bond length of CFRP. Hence, there will either be no improvements in the response characteristics or they will be insignificant when the bond length is increased beyond 300 mm as also confirmed in previous studies which indicated that after a certain bond length of CFRP, the response characteristics are almost stabilized [9,27]. Hence,

it can be confirmed that the strengthening of RHS members with 300 mm bond length of CFRP is most effective.

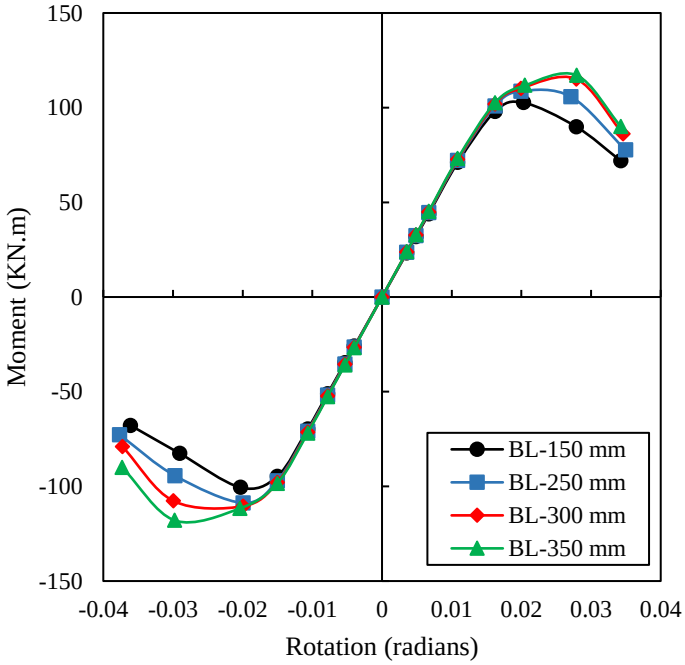

Figure 14: Moment-rotational backbone curves of CFRP strengthened RHS members with different bond lengths of CFRP

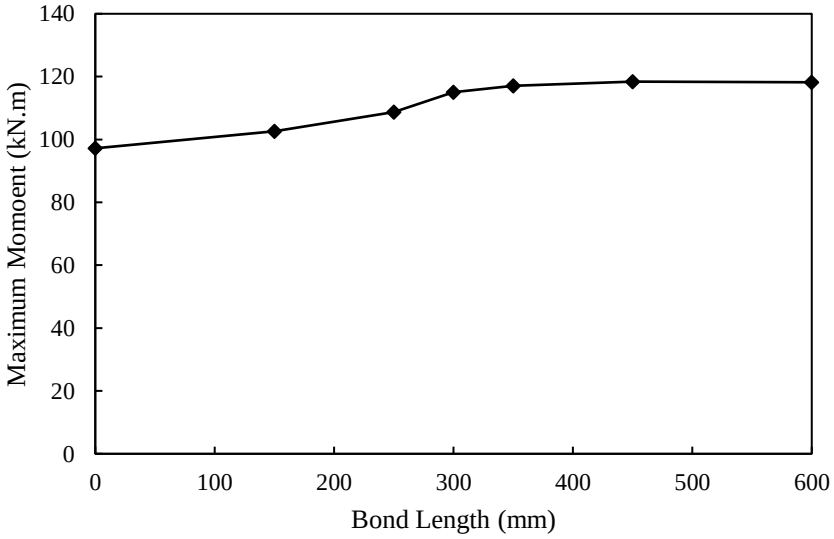

Figure 15: Maximum moment capacities of CFRP strengthened RHS members with different bond lengths of CFRP

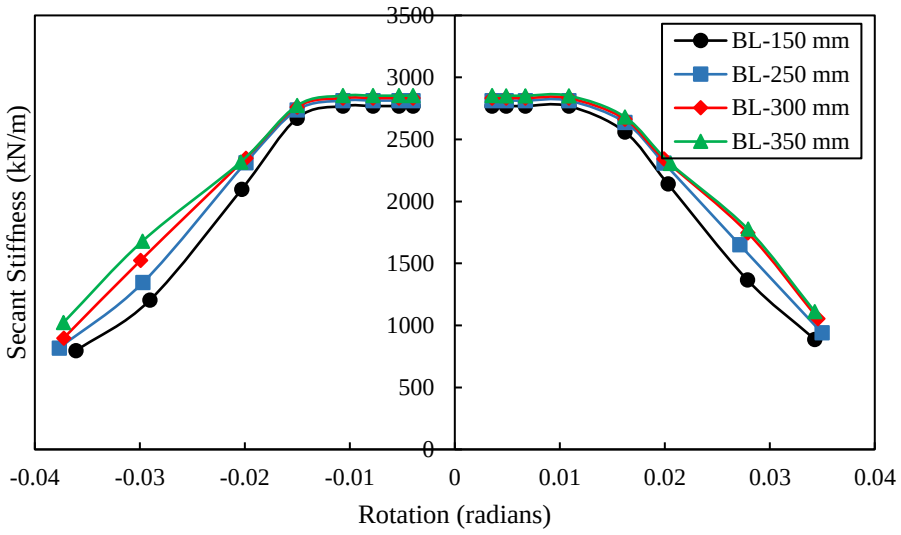

Figure 16: Secant stiffness-rotational curves of CFRP strengthened RHS members with different bond lengths of CFRP

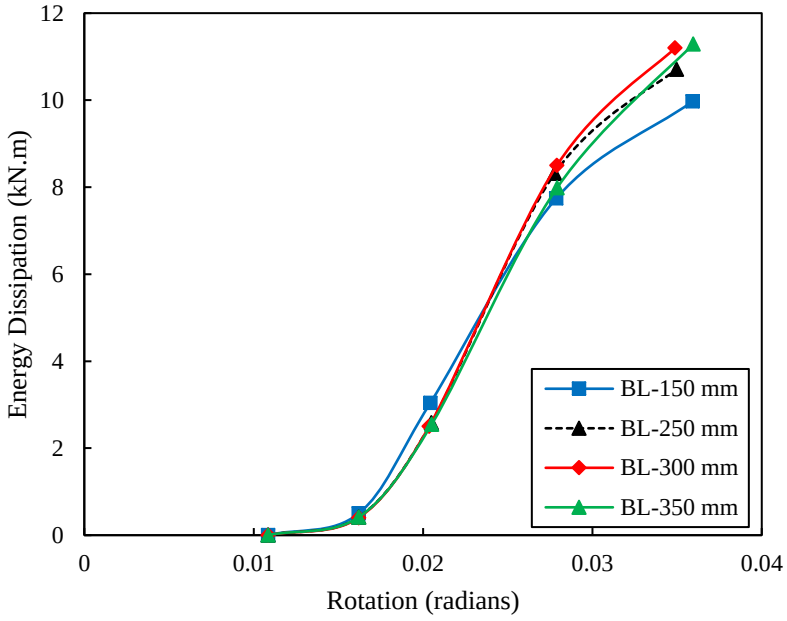

Figure 17: Energy dissipation-rotational curves of CFRP strengthened RHS members with different bond lengths of CFRP

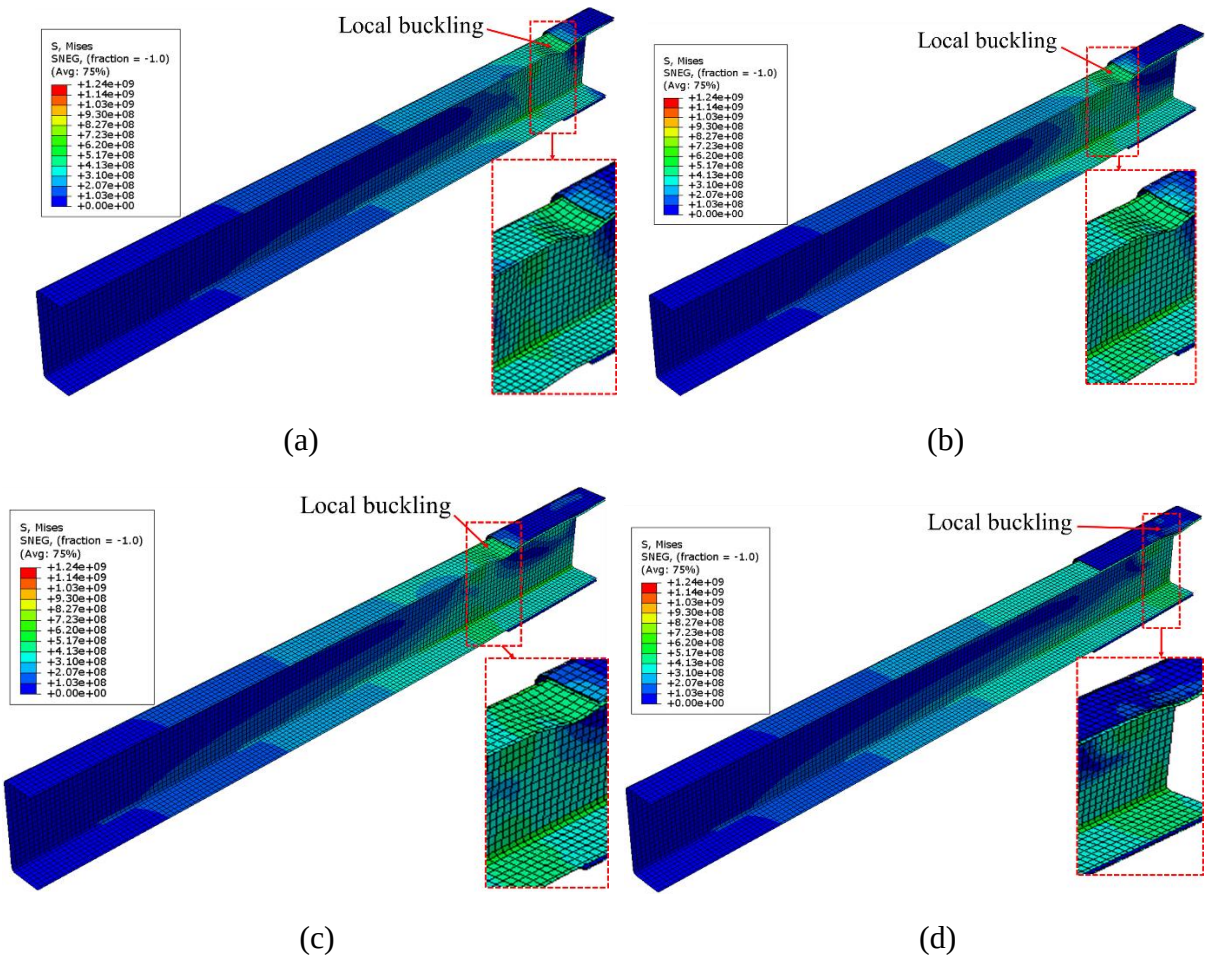

Figure 18: Failure modes of CFRP strengthened RHS members with bond lengths of (a) 150 mm (b) 250 mm (c) 300 mm and (d) 350 mm.

4.3 Effects of the number of layers of CFRP

It has been confirmed that strengthening RHS members with 300 mm bond length of CFRP is effective in enhancing its cyclic response by improving the moment-rotation hysteresis behaviour, secant stiffness and energy dissipation capacity compared to others bond lengths. Hence, only the strengthening of RHS members with 300 mm bond length will be considered for investigating the effect of the number of layers of CFRP and the other parameters. The number of CFRP layers was varied from 1 to 4 layers to investigate its effect. Moment-rotation backbone curves, maximum moment capacities, secant stiffness–rotation curves and the energy

dissipation of RHS members strengthened with number of CFRP layers from 1 to 4 are shown in Figure 19, Figure 20, Figure 21 and Figure 22.

These figures show that the different characteristics (maximum moment capacity, moment degradation, secant stiffness and energy dissipation) of CFRP strengthened RHS members improved with an increase in number of CFRP layers number from 1 layer to 4 layers and reach maximum values with 4 layers of CFRP. In addition, when the number of CFRP players are increased from 1 to 3, it is seen that the relative increments of the different characteristics are significant. But, when the number of CFRP layers is increased from 3 to 4, there are either no changes or the changes in these characteristics are insignificant.

Failure modes of CFRP strengthened RHS members with the different number of layers of CFRP are shown in Figure 23. Local buckling in the strengthened RHS members with 1 and 2 layers of CFRP can be observed to be close to the support end, while it has shifted from the support to the steel beyond the CFRP wrapped area when there are 3 or 4 layers of CFRP. Hence, 1 and 2 layers of CFRP are inadequate to provide sufficient stiffness in the support end to shift the local buckling away from the support, while 3 layers CFRP provide sufficient stiffness to shift the region of local buckling away from the support end. Further increase (beyond 3) in the number of CFRP layers showed either very little or no improvement in the different characteristics.This feature was also captured in previous experimental and numerical studies [12]. Hence, it can be confirmed that the increase in the number of layers of CFRP enhances the cyclic behaviour of CFRP strengthened RHS members. In addition, strengthening of RHS member with 3 layers of CFRP is most effective and is adequate to provide sufficient stiffness to shift the local buckling away from the support end. This parametric study will be very helpful for determining the most cost-effective number of layers of CFRP to obtain a reasonable increase in the cyclic behaviour of RHS.

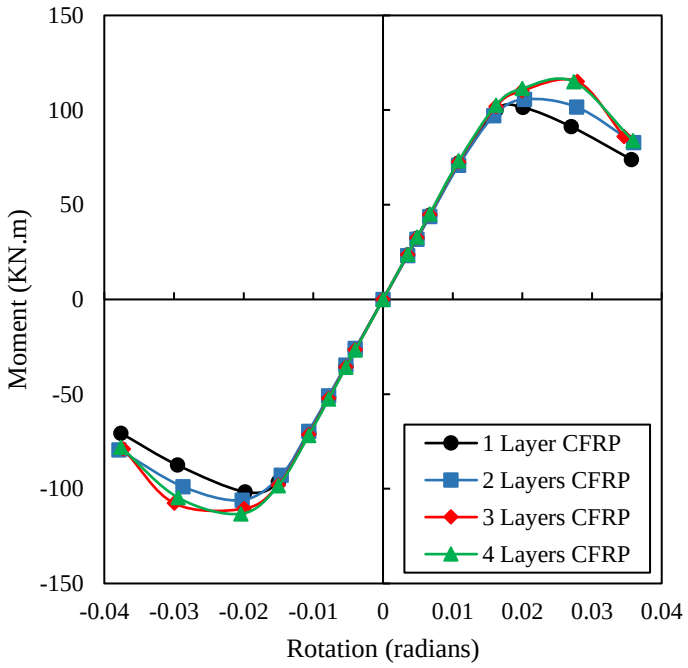

Figure 19: Moment-rotational backbone curves for CFRP strengthened RHS members with different number of layers of CFRP

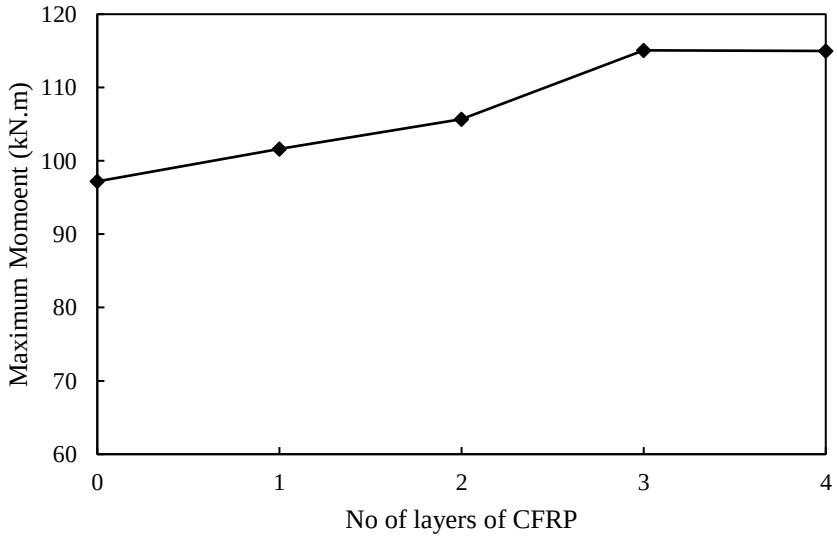

Figure 20: Maximum moment capacities of CFRP strengthened RHS members with different number of layers of CFRP

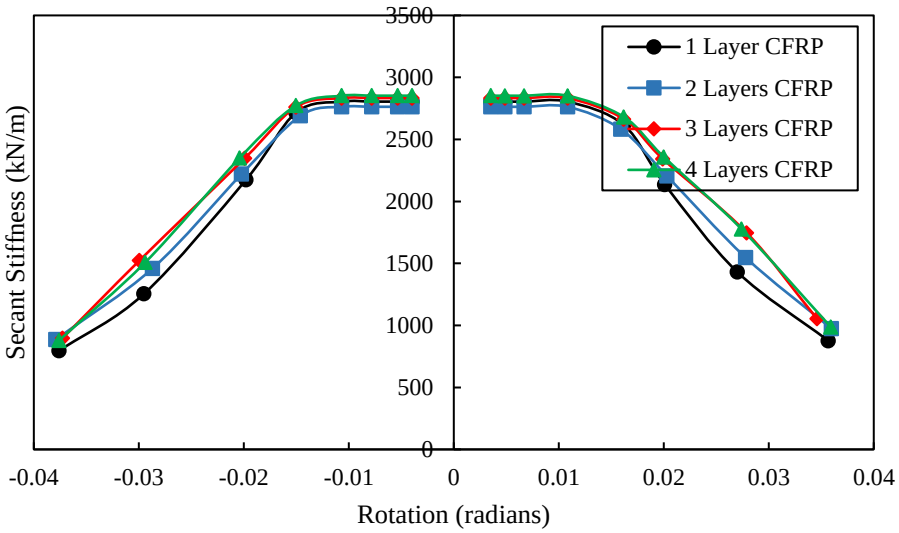

Figure 21: Secant stiffness-rotational curves for CFRP strengthened RHS members with different number of CFRP layers.

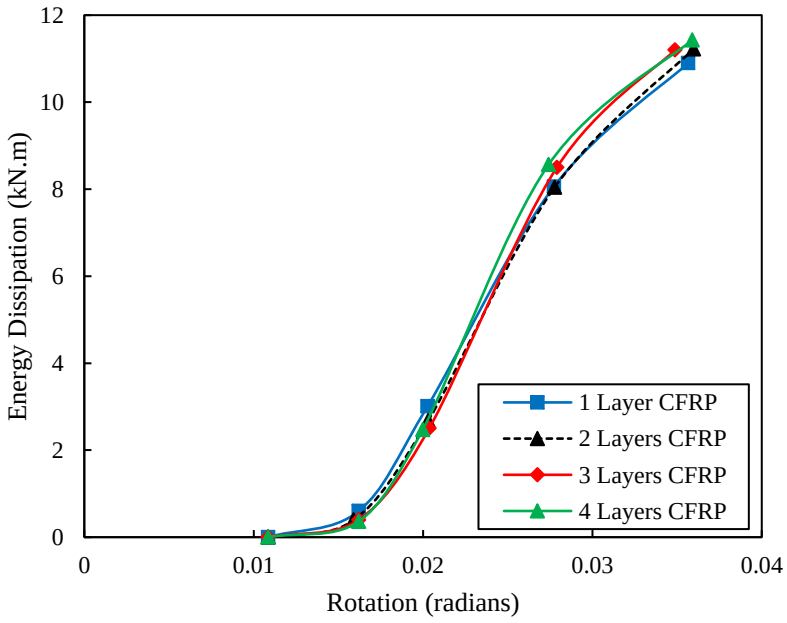

Figure 22: Energy dissipation-rotational curves of CFRP strengthened RHS members with different number of layers of CFRP

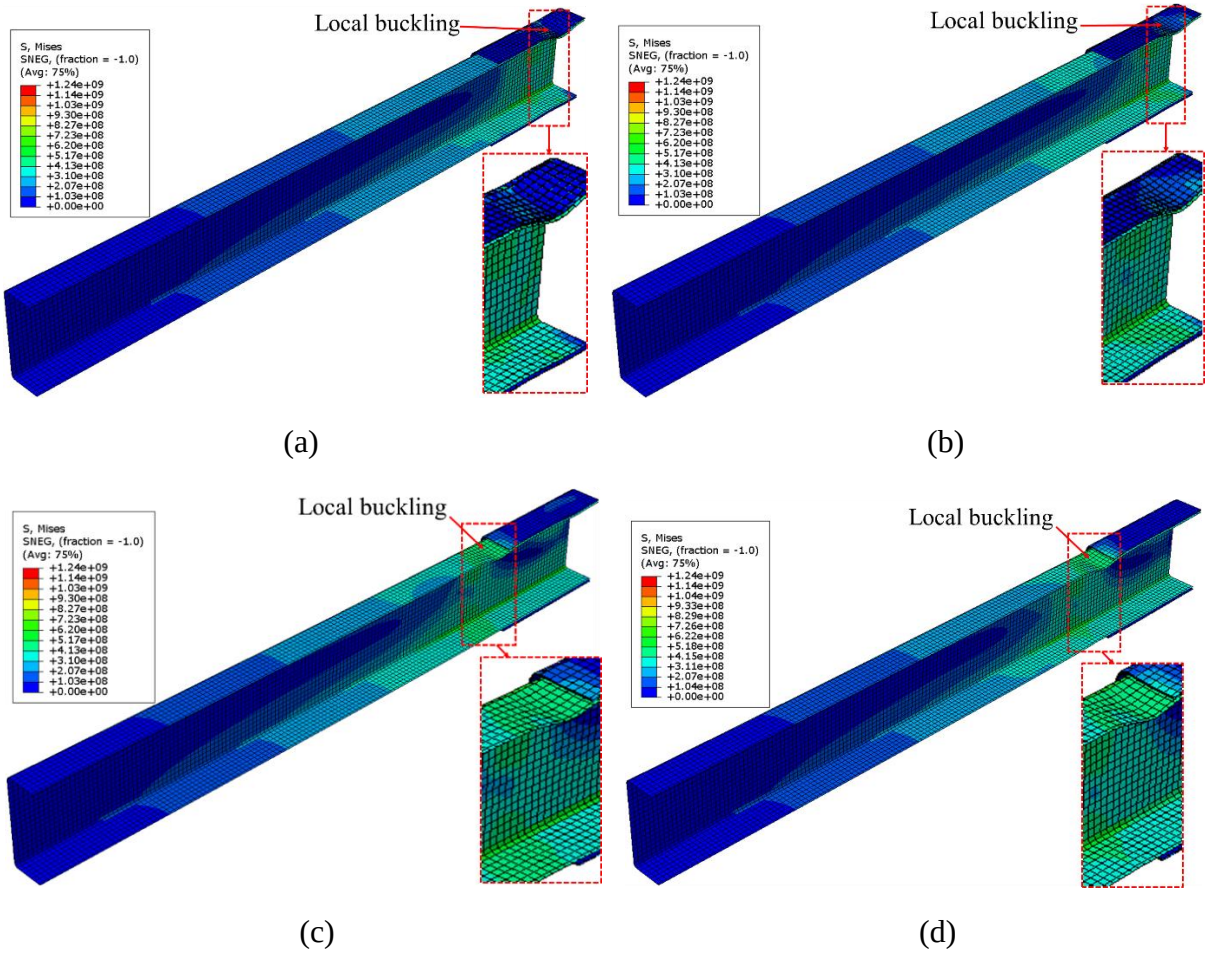

Figure 23: Failure modes of CFRP strengthened RHS members with (a) 1 layer of CFRP (b) 2 layers of CFRP (c) 3 layers of CFRP and (d) 4 layers of CFRP.

4.4 Effects of the orientation of CFRP layers

The Fiber direction of CFRP composites can play an important role in improving the structural capacity. Three more different CFRP orientations HHL, LLL and LLH along with previous orientation LHL were considered in the wrapping modelling to evaluate the effects of FRP wrapping direction. RHS members strengthened with 300 mm bond length of CFRP and 3 with layers of CFRP were considered as these optimal values were established in the previous sections. Moment-rotation hysteresis behaviour, secant stiffness and energy dissipation capabilities under cyclic loading of the CFRP strengthened RHS members with different layer orientations of CFRP are shown in Figure 24, Figure 25 and Figure 26 respectively.

These figures show that overall the RHS member strengthened with CFRP layers having HHL orientation performs slightly better than the RHS members strengthened with CFRP layers with LLL orientation in terms of moment-rotation hysteresis behaviour, secant stiffness and energy dissipation capabilities. In addition, the strengthened RHS members with CFRP layers having LHL and LLH orientations show slightly better performance compared to that with CFRP layers having HHL orientation. CFRP layers having LHL and LLH orientations have very similar effects on the strengthened RHS members in terms of all three response characteristics. Hence, both LHL and LLH orientation of CFRP layers can be used for cyclic strengthening of the RHS members from a structural application point of view. However from a theoretical perspective, the outer hoop (H) layer is weaker than the outer longitudinal (L) layer and as a result, the outer hoop layer will elongate more compared to the outer longitudinal layer. Hence, more moisture penetration might be allowed by the outer hoop layer specifically in wet environments. Therefore, in the present study, strengthening of the RHS members with the LHL CFRP layer orientation is proposed which was also recommended in a previous study on bending of CFRP strengthened steel beams [9].

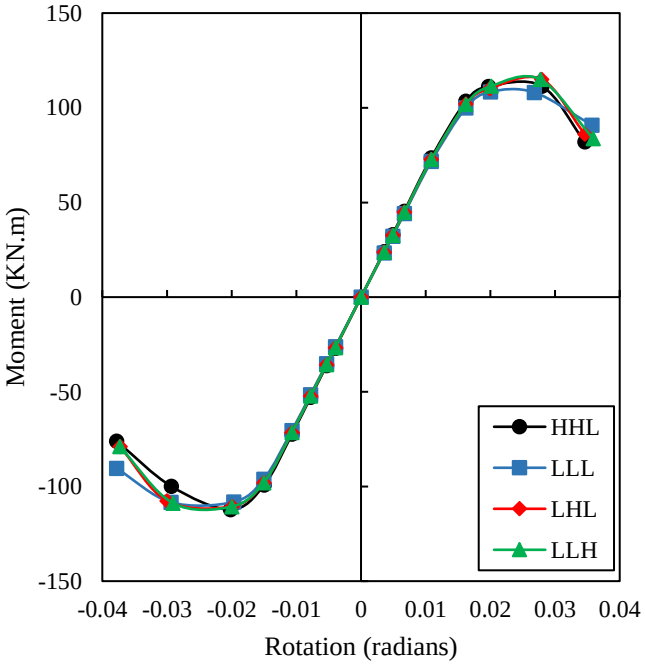

Figure 24: Moment-rotational backbone curves of CFRP strengthened RHS members with different CFRP layers orientation

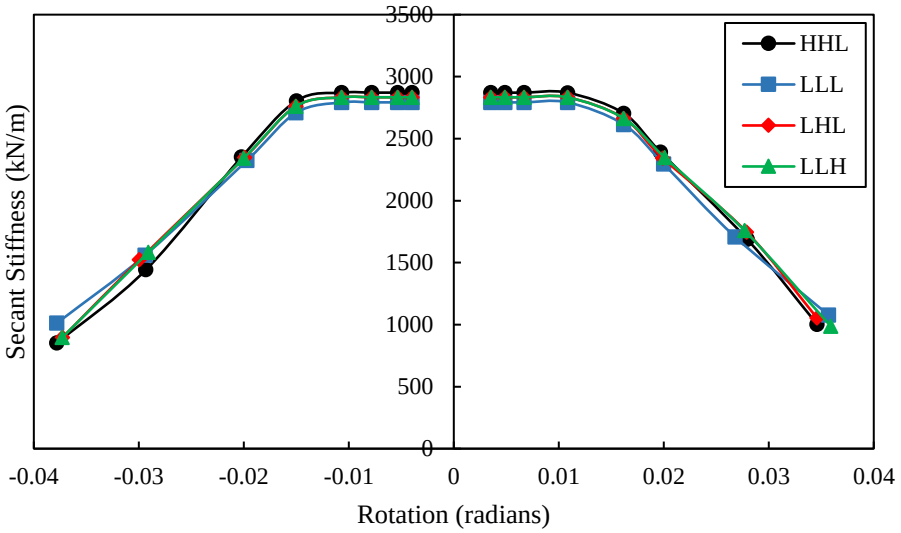

Figure 25: Secant stiffness-rotational curves of CFRP strengthened RHS members with different CFRP layers orientation

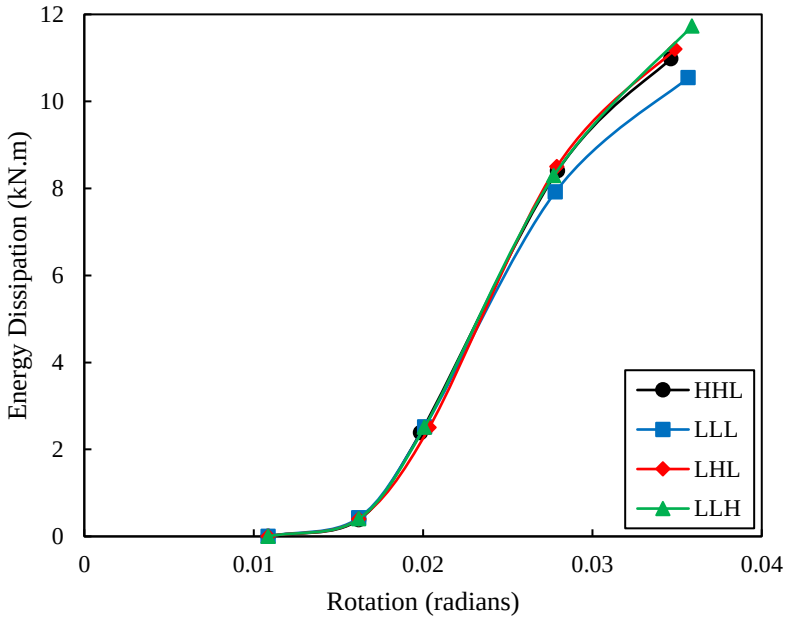

Figure 26: Energy dissipation-rotational curves of CFRP strengthened RHS members with different CFRP layers orientation

4.5 Effects of modulus of CFRP

To evaluate the effects of the modulus of CFRP on the cyclic response of CFRP strengthened RHS members under cyclic loading, RHS steel members strengthened with a normal modulus (NM) CFRP and a higher modulus (HM) CFRP along with the 300 mm bond length, 3 layers of CFRP and LHL layers orientation of CFRP are considered. The normal modulus (NM) CFRP used in previous sections is considered as the NM CFRP and the high modulus (HM) unidirectional Mbrace-CF530 CFRP, supplied by BASF chemicals, Australia, is considered as the HM CFRP. The elastic modulus, tensile strength, density and thickness of HM CFRP are 640 GPa, 2650 MPa, 2100 kg/m^3 and 0.19 mm respectively as obtained from a previous study [44]. The equivalent properties of HM CFRP composite based on a previous study [45] have been calculated and used in the present study. The calculated equivalent modulus of elasticity and tensile strength are 205 GPa and 871 MPa. The longitudinal compressive strength (20% of tensile strength), transverse tensile/compressive (10% of tensile strength) and longitudinal/transverse shear strengths (10% of tensile strength) are calculated according to Imran et al. [28]. Moreover, the values of fracture energies, 91600 N/m, 79900 N/m, 1 N/m and 1 N/m for G_{ft}, G_{fc}, G_{mc} and G_{mt} respectively, are obtained from [29] where the used CFRPs modulus of elasticity (205 GPa) was same as present equivalent modulus of elasticity.

The FE simulated cyclic responses of the CFRP strengthened RHS members with NM and HM CFRP in terms of moment-rotation hysteresis behaviour, secant stiffness and energy dissipation capabilities are presented in Figure 27, Figure 28 and Figure 29 respectively. At the initial level of rotation, the secant stiffness of the HM CFRP strengthened RHS member was slightly higher than the NM CFRP strengthened RHS member which may due to the high stiffness characteristics of HM CFRP. Apart from this, effects of the modulus of CFRP are negligible as no notable variation of moment capacity, secant stiffness and energy dissipation are found between the NM and HM CFRP strengthened RHS members. From the failure modes of CFRP

strengthened RHS with NM and HM CFRP shown in Figure 30, it can be noticed that NM CFRP is adequate to provide sufficient stiffness in the support end to shift the local buckling away from the support end and local buckling occurred in the steel section. Hence, further use of higher stiffness CFRP to provide more stiffness in the support end will not have any advantage as stiffness provided by NM CFRP is adequate. As a result, negligible variation of the structural performances is found between the NM and HM CFRP strengthened RHS members.

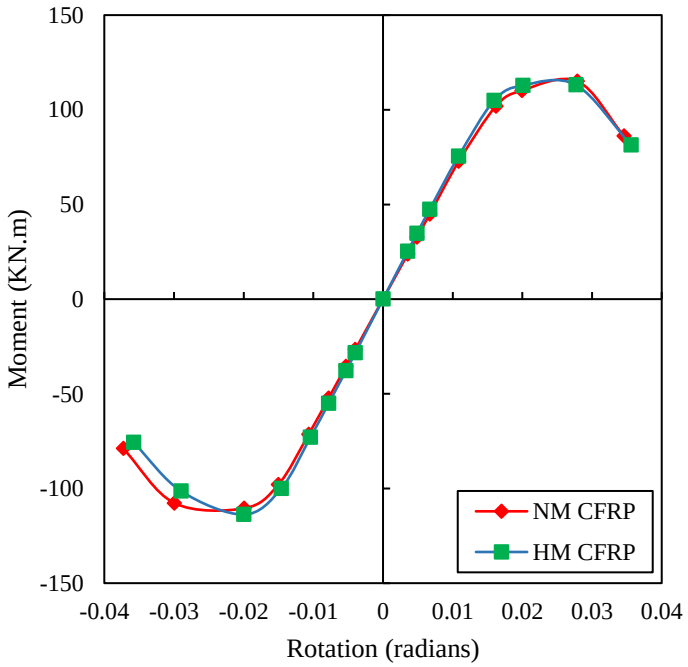

Figure 27: Moment-rotational backbone curves of CFRP strengthened RHS members with the two different moduli of CFRP

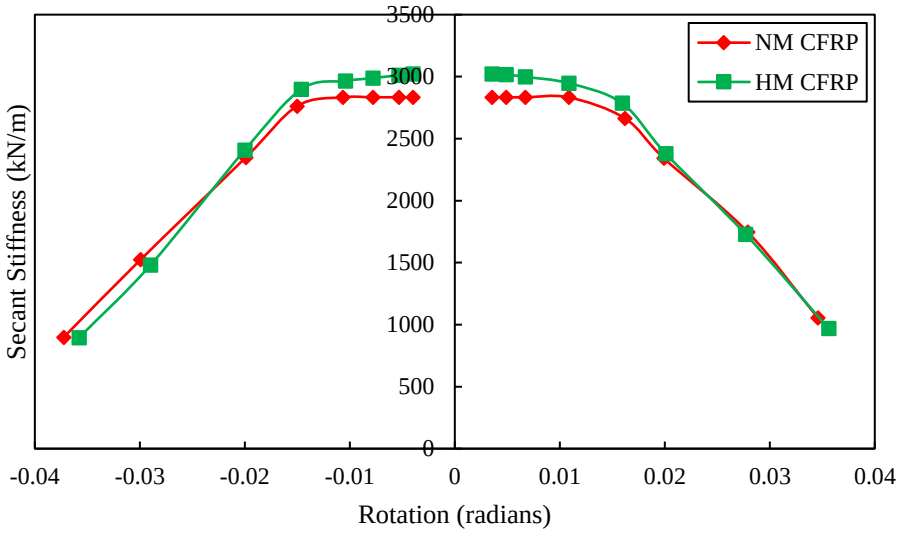

Figure 28: Secant stiffness-rotational curves of CFRP strengthened RHS members with the two different moduli of CFRP

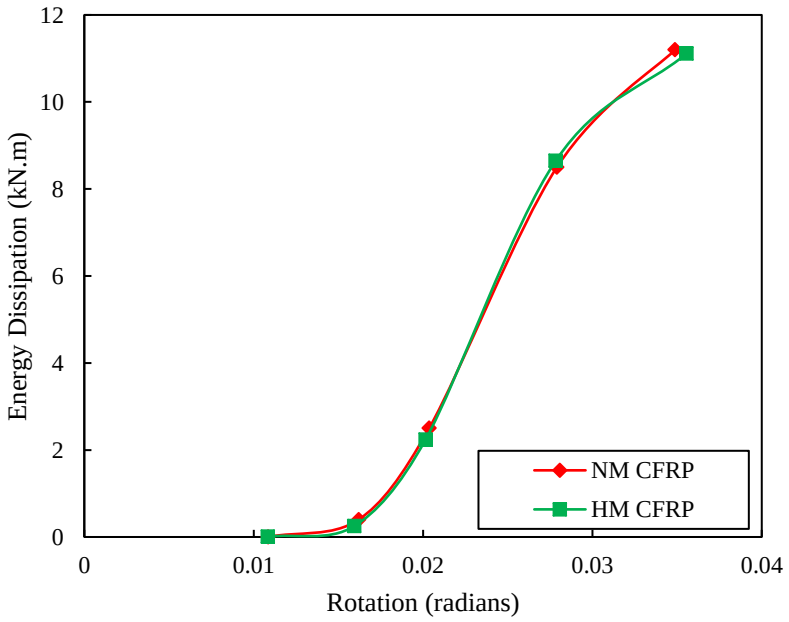

Figure 29: Energy Dissipation-rotational curves of CFRP strengthened RHS members with two different moduli of CFRP

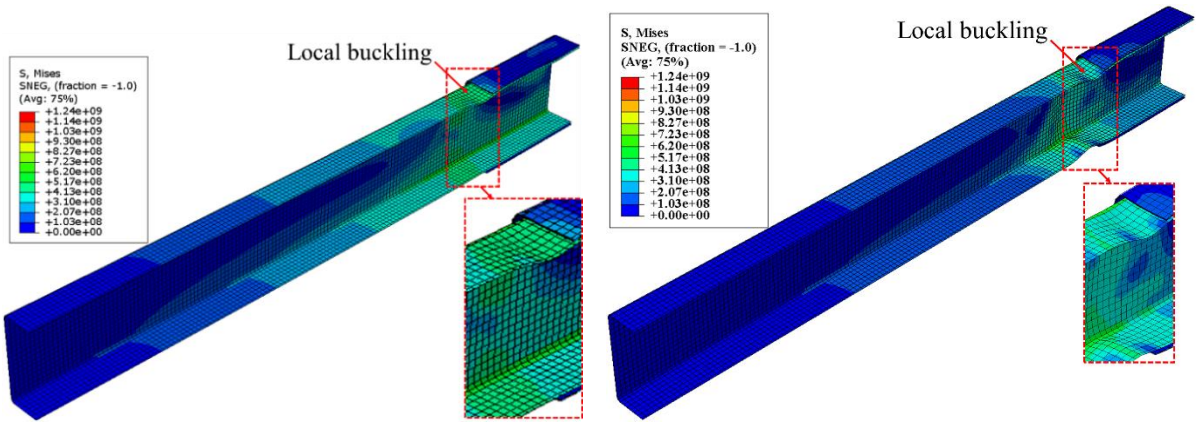

(a) (b)

Figure 30: Failure modes of CFRP strengthened RHS members with (a) NM CFRP (b) HM CFRP.

5. Conclusions

This study presents the numerical simulation and analysis of CFRP strengthened RHS steel members subjected to cyclic loading through Finite element (FE) analysis. Initially, the FE modelling techniques were validated by comparing the present results with those from available experiments. Results from the present study implied that CFRP strengthening is able to enhance the cyclic performance of RHS steel members. A detailed parametric study was also performed to evaluate the effects of section thickness, the bond length of CFRP, the number of CFRP layers, wrapping orientation of CFRP and modulus of CFRP on the structural performance of the modelled members under cyclic loading. The major observations of this research can be captured as follows:

1. The developed FE modelling technique can effectively predict the behaviour of CFRP strengthened RHS members subjected to cyclic loading. CFRP strengthened RHS steel members show better structural performance in which the moment-rotation hysteresis behaviour, secant stiffness and energy dissipating capacity are improved compared those of bare steel RHS members and confirmed the effectiveness of the CFRP strengthening technique.

2. Effectiveness of CFRP to improve the moment-rotation hysteresis behaviour, secant stiffness and energy dissipating capacity of RHS members under cyclic loading increases with the decrease in the thickness of the RHS as the ratio of CFRP thickness to RHS thickness is increased.

3. The moment-rotation hysteresis behaviour, secant stiffness and energy dissipating capacity of CFRP strengthened RHS members enhances with the increase of the bond length of CFRP up to 300 mm. However, either very little or no change is observed when the bond length is increased beyond 300 mm.

4. Strengthening the RHS with 3 layers of CFRP is most effective as the CFRP strengthened RHS members show very little or no improvement in moment-rotation hysteresis behaviour, secant stiffness and energy dissipating capacity beyond 3 layers of CFRP.

5. Both LHL and LLH CFRP layer orientations can be used for cyclic strengthening of the RHS members, but LHL CFRP layer orientation has been recommended due to its theoretical advantage in wet environment.

6. The effects of the modulus of CFRP is negligible and no notable variation in cyclic performance was observed between the NM and HM CFRP strengthened RHS members as the NM CFRP is adequate to provide the sufficient stiffness.

Acknowledgment

The authors would like to thank, Queensland University of Technology (QUT) for providing support (computer, software for analysis) to carry out the work reported in this paper.

Data Availability Statement

The raw/processed data required to reproduce these findings cannot be shared at this time as the data also forms part of an ongoing study.

References

[1] J. Wardenier, J.A. Packer, X.L. Zhao, G.J. Van der Vegte, Hollow sections in structural applications, Bouwen met Staal Rotterdam,, The Netherlands, 2002.

[2] D. Guha-Sapir, R. Below, P. Hoyois, EM-DAT: International disaster database, Cathol. Univ. Louvain Brussels, Belgium. (2015).

[3] ANSI/AISC 341-16, Seismic Provisions for Structural Steel Buildings, Am. Inst. Steel Constr. (2016) 402. doi:111.

[4] M. V. Seica, J.A. Packer, FRP materials for the rehabilitation of tubular steel structures, for underwater applications, Compos. Struct. 80 (2007) 440–450. doi:10.1016/j.compstruct.2006.05.029.

[5] L.C. Hollaway, J.-G. Teng, Strengthening and rehabilitation of civil infrastructures using fibre-reinforced polymer (FRP) composites, Woodhead Publishing, Sawston, Cambridge, UK, 2008.

[6] C. Batuwitage, S. Fawzia, D.P. Thambiratnam, T. Tafsirojjaman, R. Al-Mahaidi, M. Elchalakani, CFRP-wrapped hollow steel tubes under axial impact loading, in: Tubul. Struct. XVI Proc. 16th Int. Symp. Tubul. Struct. (ISTS 2017, 4-6 December 2017, Melbourne, Aust., CRC Press, 2017: p. 401.

[7] X.L. Zhao, L. Zhang, State-of-the-art review on FRP strengthened steel structures, Eng. Struct. 29 (2007) 1808–1823. doi:10.1016/j.engstruct.2006.10.006.

[8] J.G. Teng, J.F. Chen, S.T. Smith, L. Lam, Behaviour and strength of FRP-strengthened RC structures: a state-of-the-art review, Proc. Inst. Civ. Eng. - Struct. Build. 156 (2003) 51–62. doi:10.1680/stbu.2003.156.1.51.

[9] M.H. Kabir, S. Fawzia, T.H.T. Chan, J.C.P.H. Gamage, J.B. Bai, Experimental and numerical investigation of the behaviour of CFRP strengthened CHS beams subjected to bending, Eng. Struct. 113 (2016) 160–173. doi:10.1016/j.engstruct.2016.01.047.

[10] M.I. Alam, S. Fawzia, T. Tafsirojjaman, X.L. Zhao, FE modeling of FRP strengthened CHS members subjected to lateral impact, in: Tubul. Struct. XVI Proc. 16th Int. Symp. Tubul. Struct. (ISTS 2017, 4-6 December 2017, Melbourne, Aust., CRC Press, 2017: p. 409.

[11] Tafsirojjaman, S. Fawzia, D. Thambiratnam, Enhancement Of Seismic Performance Of Steel Frame Through CFRP Strengthening, Procedia Manuf. 30 (2019) 239–246. doi:10.1016/j.promfg.2019.02.035.

[12] T. Tafsirojjaman, S. Fawzia, D. Thambiratnam, X.L. Zhao, Seismic strengthening of rigid steel frame with CFRP, Arch. Civ. Mech. Eng. 19 (2019) 334–347. doi:10.1016/j.acme.2018.08.007.

[13] N.D. Fernando, Bond behaviour and debonding failures in CFRP-strengthened steel members, The Hong Kong Polytechnic University, 2010.

[14] K.A. Harries, A.J. Peck, E.J. Abraham, Enhancing stability of structural steel sections using FRP, Thin-Walled Struct. 47 (2009) 1092–1101. doi:10.1016/j.tws.2008.10.007.

[15] M.I. Alam, S. Fawzia, Numerical studies on CFRP strengthened steel columns under transverse impact, Compos. Struct. 120 (2015) 428–441.

doi:10.1016/j.compstruct.2014.10.022.

[16] H. Nakamura, W. Jiang, H. Suzuki, Maeda, T. Irube, Experimental study on repair of fatigue cracks at welded web gusset joint using CFRP strips, Thin-Walled Struct. 47 (2009) 1059–1068. doi:10.1016/j.tws.2008.10.016.

[17] T. CHEN, Q.-Q. YU, X.-L. GU, X.-L. ZHAO, Study on Fatigue Behavior of Strengthened Non-Load-Carrying Cruciform Welded Joints Using Carbon Fiber Sheets, Int. J. Struct. Stab. Dyn. 12 (2012) 179–194. doi:10.1142/S0219455412004586.

[18] Z.-G. Xiao, X.-L. Zhao, CFRP repaired welded thin-walled cross-beam connections subject to in-plane fatigue loading, Int. J. Struct. Stab. Dyn. 12 (2012) 195–211.

[19] N. Photiou, L.C. Hollaway, M.K. Chryssanthopoulos, Strengthening Of An Artificially Degraded Steel Beam Utilising A Carbon/Glass Composite System, Adv. Polym. Compos. Struct. Appl. Constr. ACIC 2004. 20 (2004) 274–283. doi:10.1016/B978-1-85573-736-5.50030-3.

[20] J. Haedir, M.R. Bambach, X.L. Zhao, R.H. Grzebieta, Strength of circular hollow sections (CHS) tubular beams externally reinforced by carbon FRP sheets in pure bending, Thin-Walled Struct. 47 (2009) 1136–1147. doi:10.1016/j.tws.2008.10.017.

[21] T. Tafsirojjaman, S. Fawzia, D. Thambiratnam, X.L. Zhao, Behaviour of CFRP strengthened CHS members under monotonic and cyclic loading, Compos. Struct. 220 (2019) 592–601. doi:10.1016/j.compstruct.2019.04.029.

[22] SIMULIA, ABAQUS 6.19, ABAQUS Anal. Theory Manuals, SIMULIA, Dassault Systèmes, Realis. Simulation, Provid. RI, USA. (2019).

[23] M. Fadden, Cyclic Bending Behavior of Hollow Structural Sections and their Application in Seismic Moment Frame Systems., University of Michigan, Ann Arbor, 2013.

[24] AISC, Manual of steel construction, 14th editi (2011).

[25] M. Fadden, J. McCormick, Finite element model of the cyclic bending behavior of hollow structural sections, J. Constr. Steel Res. 94 (2014) 64–75. doi:10.1016/j.jcsr.2013.10.021.

[26] S. Fawzia, X.L. Zhao, S. Rizkalla, Bond characteristics between CFRP and steel plates in double strap joints, Int. J. Adv. Steel Constr. 1 (2005) 17–27.

[27] M.I. Alam, S. Fawzia, X. Liu, Effect of bond length on the behaviour of CFRP strengthened concrete-filled steel tubes under transverse impact, Compos. Struct. 132 (2015) 898–914. doi:10.1016/j.compstruct.2015.06.065.

[28] M. Imran, M. Mahendran, P. Keerthan, Experimental and numerical investigations of CFRP strengthened short SHS steel columns, Eng. Struct. 175 (2018) 879–894. doi:10.1016/j.engstruct.2018.08.042.

[29] M.H. Kabir, S. Fawzia, T.H.T. Chan, M. Badawi, Numerical studies on CFRP strengthened steel circular members under marine environment, Mater. Struct. 49 (2016) 4201–4216. doi:10.1617/s11527-015-0781-5.

[30] J.G. Teng, D. Fernando, T. Yu, Finite element modelling of debonding failures in steel beams flexurally strengthened with CFRP laminates, Eng. Struct. 86 (2015) 213–224.

doi:10.1016/j.engstruct.2015.01.003.

[31] L. De Lorenzis, D. Fernando, J.G. Teng, Coupled mixed-mode cohesive zone modeling of interfacial debonding in simply supported plated beams, Int. J. Solids Struct. 50 (2013) 2477–2494. doi:10.1016/j.ijsolstr.2013.03.035.

[32] M.F.S.F. De Moura, J.A.G. Chousal, Cohesive and continuum damage models applied to fracture characterization of bonded joints, Int. J. Mech. Sci. 48 (2006) 493–503. doi:10.1016/j.ijmecsci.2005.12.008.

[33] Y. Yang, H. Biscaia, C. Chastre, M.A.G. Silva, Bond characteristics of CFRP-to-steel joints, J. Constr. Steel Res. 138 (2017) 401–419. doi:10.1016/j.jcsr.2017.08.001.

[34] Y. Yang, M.A.G. Silva, H. Biscaia, C. Chastre, Bond durability of CFRP laminates-to-steel joints subjected to freeze-thaw, Compos. Struct. 212 (2019) 243–258. doi:10.1016/j.compstruct.2019.01.016.

[35] M.M.R. Dawood, Bond characteristics and environmental durability of CFRP materials for strengthening steel bridges and structures, North Carolina State University, 2008.

[36] P. Naghipour, J. Schneider, M. Bartsch, J. Hausmann, H. Voggenreiter, Fracture simulation of CFRP laminates in mixed mode bending, Eng. Fract. Mech. 76 (2009) 2821–2833. doi:10.1016/j.engfracmech.2009.05.009.

[37] M.L. Benzeggagh, M. Kenane, Measurement of mixed-mode delamination fracture toughness of unidirectional glass/epoxy composites with mixed-mode bending apparatus, Compos. Sci. Technol. 56 (1996) 439–449.

[38] Z. Hashin, Failure Criteria for Unidirectional FibreComposites, J. Appl. Mech. 47 (1980) 329–334.

[39] Z. Hashin, A. Rotem, A fatigue failure criterion for fiber reinforced materials, J. Compos. Mater. 7 (1973) 448–464.

[40] M. Lesani, M.R. Bahaari, M.M. Shokrieh, Numerical investigation of FRP-strengthened tubular T-joints under axial compressive loads, Constr. Build. Mater. 53 (2014) 243–252. doi:10.1016/j.conbuildmat.2013.11.097.

[41] A. Faggiani, B.G. Falzon, Predicting low-velocity impact damage on a stiffened composite panel, Compos. Part A Appl. Sci. Manuf. 41 (2010) 737–749. doi:10.1016/j.compositesa.2010.02.005.

[42] D. Mostofinejad, N. Moshiri, Compressive Strength of CFRP Composites Used for Strengthening of RC Columns: Comparative Evaluation of EBR and Grooving Methods, J. Compos. Constr. 19 (2014) 04014079. doi:10.1061/(asce)cc.1943-5614.0000545.

[43] F. Nunes, J.R. Correia, N. Silvestre, Structural behavior of hybrid FRP pultruded beams: Experimental, numerical and analytical studies, Thin-Walled Struct. 106 (2016) 201–217. doi:10.1016/j.tws.2016.05.004.

[44] S. Fawzia, R. Al-Mahaidi, X.L. Zhao, S. Rizkalla, Strengthening of circular hollow steel tubular sections using high modulus CFRP sheets, Constr. Build. Mater. 21 (2007) 839–845.

[45] S. Fawzia, R. Al-Mahaidi, X.L. Zhao, Experimental and finite element analysis of a double strap joint between steel plates and normal modulus CFRP, Compos. Struct. 75

(2006) 156–162. doi:10.1016/j.compstruct.2006.04.038.